INVESTIGATING THE IMPACT OF VISCOELASTICITY ON γδ T CELL MIGRATORY BEHAVIORS FOR ENHANCED TUMOR INFILTRATION

A thesis presented by

Michelle Jia Chang

Presented to

the Faculty of the
Harvard John A. Paulson School of Engineering and Applied Sciences

in partial fulfillment of the requirements for
the Bachelor of Arts degree in
Biomedical Engineering (A.B)

Faculty Advisor: Prof. David Mooney, Ph.D.

Harvard University

Cambridge, MA

May 27, 2026

Honor Code

In submitting this thesis to Harvard John A. Paulson School of Engineering and Applied Sciences in partial fulfillment of the requirements for the degree with honors of Bachelor of Arts, I affirm my awareness of the standards of the Harvard College Honor Code.

Name: Michelle Chang

Signature: *Michelle Chang*

The Harvard College Honor Code Members of the Harvard College community commit themselves to producing academic work of integrity – that is, work that adheres to the scholarly and intellectual standards of accurate attribution of sources, appropriate collection and use of data, and transparent acknowledgement of the contribution of others to their ideas, discoveries, interpretations, and conclusions. Cheating on exams or problem sets, plagiarizing or misrepresenting the ideas or language of someone else as one's own, falsifying data, or any other instance of academic dishonesty violates the standards of our community, as well as the standards of the wider world of learning and affairs.

Table of Contents

Figures and Tables

Acknowledgements

I would like to begin by expressing my deepest gratitude to my research mentor, **Favour Obuseh,** for his willingness to take me on and his unwavering support in helping me complete this project. Favour has always been "the absolute rock," oftentimes encouraging me toward a potential answer or solution, but never giving them away. Instead, he continues to challenge me everday, pushing me to question and explore my data and assumptions. Ultimately, Favour has made and continues to make me a better scientist everyday.

Secondly, I would like to thank **Professor David Mooney** for introducing me to biomaterials and biomechanics through BE125 and for giving me the opportunity to be a part of his lab. I am eternally grateful for Professor Mooney in trusting and believing in me to not only support me in my own research project, but also in all my future career ambitions. The positive, collaborative environment Professor Mooney has cultivated in this lab has inspired me in such a way that I would never have thought that I would be walking away feeling so empowered, passionate, and determined to continue research.

Thirdly, I would like to thank the entirety of the Mooney lab. My time in this lab has genuinely been one of the most transformative experiences in my life, shaping not only my scientific thinking, but also my confidence as an independent researcher. Thank you to **Dr. Wei-Hung Jung** for teaching me how to use the rheometer, track cell movement through ImageJ, using the confocal microscope, and giving me little motivational snippets as this project progressed. Thank you to **Blake Hanan, Kyle Ruark,** and **Tania To** for helping me find reagents, letting me in when I lock myself out on the stairs, and having endless amounts of energy to talk about all things in life. Thank you to **Leah Lourenco** for the great company during every single cell isolation, incubation, and everything in between.

In addition, I would like to thank my parents and brother, **Christine Chang, Kenneth Chang,** and **Edward Chang,** for their endless support, love, and continuous belief in me. I am eternally grateful for my mother, who never fails to pick up the phone to chat about my wins, losses, and everything in between. I owe special thanks to my father for modeling what it means to think critically and establishing that ambitious mentality and drive of mind over matter. I would also like to establish my sincere gratitude to my little brother who experiences and receives my texts about "the biggest crashout of my life" every week.

Finally, I would like to thank all of my lovelies that have been a lifeline to sanity and a village of support. I am fortunate to have my dearest roommate **Ally Ah Cook** who never says no to a cafe work session, accompanies me to Solidcore, and for always being there for me through thick and thin. Thank you to **Alan Yu** who helps me debug the most obvious red errors that I always get stuck on. In addition, I offer my sincere thanks to **Vivian Tien** and **Mrs. Leslie,** for being that spark that ignited my interest in STEM and for all the introspective conversations. Thank you to my friends **Sarah**, **Dian, Ciera, Haley, Joey, Eileen and Dhriti** for always bringing their most positive energy into my life.

Ultimately, I am the person I am today, because each and every person here has continuously chosen me, challenged me, and believed in me each step of the way. As my time at Harvard comes to an end, I have no words to express the immense gratitude of the investment all my mentors, friends, and families have poured into me. Beyond this thesis and beyond Harvard, I carry that investment with me, and I hope to honor it by continuing to grow, to lead with curiosity and integrity, and to strive to be the best version of myself for each and every one of you.

List of Contributions

This thesis is based on the dissertation study of PhD candidate Favour Obuseh from the David Mooney Lab. Favour was the primary designer of the wet lab component of this lab and helped me brainstorm and edit my experimental design. Former PhD student Kwasi Adu-Berchie designed the tunable collagen hydrogel system used to encapsulate cells in this project. Furthermore, postdoctoral fellow, Dr. Wei-Hung Jung, assisted in live cell imaging, cell-staining, and rheology. I also received assistance from Leah Lourenco (Harvard Class of 2026 in the Bioengineering department and part of the Mooney Lab), in running my plates through the flow cytometer. These individuals and their contributions were all crucial in the completion of this thesis.

Abstract

Adoptive T cell therapies are an emerging area of immunotherapy that have shown promise in treating cancer, especially blood-based tumors and melanomas. Yet, their efficacy in solid tumors remains limited. Most studies have primarily used alpha beta (αβ) T cells which are restricted by MHC class presentation. This allows some tumors to evade immune detection. Recent attention has shifted toward gamma delta (γδ) T cells, a small but functionally significant subset of T cells that bridge innate and adaptive immunity. Their MHC-independent antigen recognition and cytotoxic response capabilities position them as promising candidates for adoptive immunotherapies. While *γδ* T cells have been used in a variety of clinical trials globally, *γδ* T cells still have limited efficacy in attacking solid tumors, primarily due to low tissue migration and residency. Emerging research suggests that mechanical cues in the microenvironment can influence T cell phenotype and function. In this paper, we hypothesize that mechanical modulation of the culture environment can promote a more tissue-adapted γδ T cell state. Using a collagen type I hydrogel platform with independently tunable stiffness and viscoelasticity, we encapsulated γδ T cells and assessed phenotype and motility by flow cytometry and time-lapse imaging. We found that viscoelastic, fast-relaxing hydrogels enhance γδ T-cell migration, as evidenced by increased mean squared displacement and average speed over time. In parallel, we observe increased expression of the activation and stress-associated receptors PD1 and NKG2D. These results suggest that engineering the mechanical properties of the cell culture environment can modulate γδ T-cell migratory and activation states with implications for improving their efficacy in solid tumor immunotherapy.

Chapter One: Introduction

1.1 Significance of Work

Cancer is a global health concern, causing 10 million deaths and 19.3 million new cases each year. Solid tumors account for 90% of these cases (Ng et al., 2023). Despite notable advances in cancer treatment, cancer patients have no guaranteed solutions. Specifically, the 20-, 10-, and 5-year survival rate of patients diagnosed with any malignant tumor falls around 50%, 57%, and 62% (Sakr et al., 2023). Currently, the main forms of treatment include chemotherapy, radiation, and surgery. However, these approaches not only lack the ability to selectively attack cancer cells, but also may lead to drug-related, systemic toxicities (Victor et al., 2022).

Over the past half-century, a rapidly expanding field of research has focused on stimulating and enhancing the immune system to promote cancer immunosurveillance. Among these advances, adoptive T cell therapy (ACT) has emerged as a powerful immunotherapeutic approach in which a patient's own T cells are re-engineered ex vivo and reinfused to target and eliminate cancer cells. Studies have shown that this has been effective in treating blood-based cancers, yet its efficacy in addressing solid tumors continues to be limited (Olson et al., 2023). Currently, $\alpha\beta$ T cells, the primary type of T lymphocytes, are the most commonly used. However, because $\alpha\beta$ T cells are restricted by MHC class I-mediated antigen presentation, many solid cancer cells can escape the immune system through antigen shedding or mutation (Dobosz et al., 2019).

Recent studies have shifted toward exploring the use of gamma delta T cells ($\gamma\delta$ T cells), a unique subset of T lymphocytes that function independently of the major histocompatibility complex (MHC). Specifically, $\gamma\delta$ T cells can recognize stress antigens produced by diseased

cells, promoting cytokine production and activating other immune cells (Lawand et al., 2017). Despite these promising characteristics, current clinical studies suggest that γδ T cells often exhibit limited penetration into the tissue microenvironment of solid tumors, reducing their therapeutic effectiveness. This limitation highlights the need to better understand the factors that regulate γδ T cell migration and tissue residency.

Emerging studies have suggested that mechanical cues can influence T cell phenotype and function through cellular mechanosensing pathways (Adu-Berchie et al., 2023). Biomaterials such as collagen and alginate can be used to create tissue-mimetic hydrogels that replicate aspects of the extracellular matrix. The biophysical features of these gels, including viscoelasticity and stiffness, provide mechanical signals that T cells can sense and respond to, ultimately altering their phenotype and functional behavior.

This thesis explores the use of γδ T cells as an alternative strategy for treating solid tumors. In particular, this work investigates how the viscoelastic properties of collagen hydrogels influence γδ T cell behavior, focusing on the development of tissue-resident phenotypes and changes in migrational patterns. By exploring how viscoelastic cues regulate γδ T cell migration, this study presents initial steps toward improving adoptive T cell therapies by promoting tissue residency and enhancing the ability of γδ T cells to penetrate solid tumor microenvironments.

1.2 Hypothesis

We hypothesize that by fine-tuning the mechanical properties of tissue-mimetic hydrogels and embedding $\gamma\delta$ T cells, we can alter the migratory patterns of $\gamma\delta$ T cells to exhibit a tissue-adapted state.

1.3 Specific Aims

To test this hypothesis, this research experiment was guided by the following aims:

1) Select optimal elasticity of collagen hydrogel
2) Assess the effects of the biomechanical environment on the migration patterns of $\gamma\delta$ T cells at two different time points by encapsulating cells into collagen hydrogels with distinct viscoelastic profiles: highly elastic (slow-relaxing) and viscoelastic (fast-relaxing) at two different time points: Day 0 and Day 5
3) Assess the effects of the biomechanical environment on the phenotypes of $\gamma\delta$ T cells post-encapsulation

Chapter Two: Background and Literature Review

2.1 The Solid Tumor Microenvironment

A solid tumor is a heterogenous, abnormal mass of cells caused by uncontrolled growth (Mosaffa et al., 2025). Tumor progression is not driven by malignant cells alone, but also strongly influenced by the tumor microenvironment (TME). The TME is a complex, continuously evolving system that regulates interactions between tumor cells and surrounding stromal, immune, and vascular components (Anderson et al., 2020). Specifically, the tumor microenvironment can alter molecular, cellular, and physical changes to create an environment with altered nutritional availability and cell signaling.

Collectively, these changes establish a metabolically stressed and immunosuppressive environment that drives disease progression. One hallmark of the TME and tumor progression is hypoxia, which results in the secretion of hypoxia-inducible factors (HIFs). This promotes angiogenesis within the tumor to restore oxygen and nutrient supply, while contributing to immune cell exhaustion by promoting a dysfunctional, hypoactive state in T cells (Hu et al., 2022). Furthermore, the TME can also upregulate the secretion of tumor growth factors, such as vascular endothelial growth factor (VEGF), and immunosuppressive cytokines, such as IL-6, IL-10, and TGFβ (Bilotta et al., 2022). These cytokines can induce T regulatory (Treg) cell differentiation, while recruiting circulating Tregs, suppressing anti-tumor immunity. In addition to the TME immune suppression, direct tumor to T cell interactions can inhibit immune response through the overexpression of inhibitory receptors such as PD1/PD-L1 (Baruch et al., 2017).

The tumor microenvironment (TME) can be broadly classified into three immunological states based on the presence and function of immune cells within the tumor: hot, cold, and an

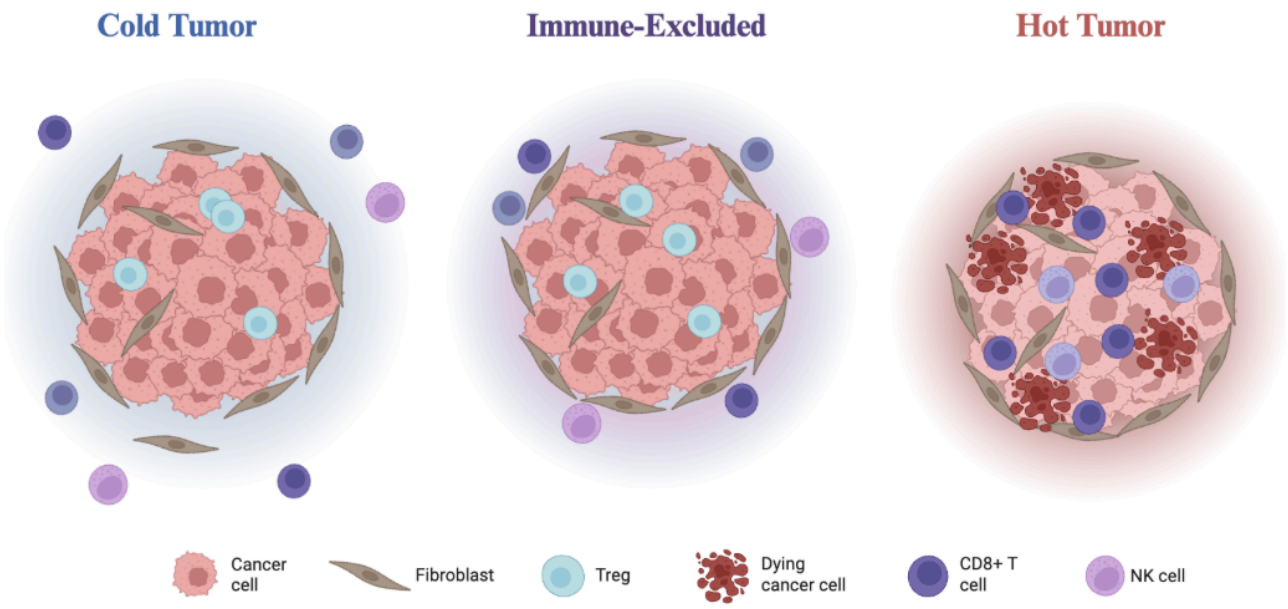

Figure 1. Overview of TME Immunological State. Cold tumors have minimal immune cell infiltration and tumor death (left). Immune-excluded cells recruit immune cells to the tumor, but lack the ability to penetrate (middle). Hot tumors exhibit a strong immune response with increased tumor cell death (right). Adapted from BioRender (2026). Original Template available at: BioRender Cold vs Hot Tumors.

intermediate state known as immune-excluded (Wu et. al., 2024). A hot tumor is characterized as a TME that has a high degree of T cell, NK cell, and B cell infiltration. The proliferation and activation of these immune cells are derived from the immune activating factors released by tumors. Typically, hot tumors respond well to immunotherapy and leads to a positive prognosis. In contrast, a cold tumor is characterized by few T cell, NK cell, and B cell infiltration, due to the activation of immunosuppressive pathways of immune checkpoints such as PD1/PD-L1 and CTLA-4 (Wang et al., 2023). Additionally, there is a more nuanced, intermediate category known as immune-excluded. In this state, anti-tumor lymphocytes are directed toward the tumor, however, they lack an ability to enter the tumor, remaining confined to the outer regions of the tumor (Wu et al., 2024). This barrier could be attributed to the lack of signals attracting these cells, such as the chemokines CKCL9, CXCL10, CXCL11, CXCL13, and CX3C chemokines

(Nagarsheth et al., 2017). Both cold and immune-excluded TMEs greatly hinder the efficacy of immunotherapies.

Ultimately, it is important to note that these TME states are not fixed, but can evolve. Nevertheless, the success of immunotherapies depend on effective immune activation, penetration, and functionality within the TME.

2.2 Adoptive T cell Therapies

Adoptive T cell therapies (ACT) is an emerging immunotherapy that bolsters the immune response against cancer. Specifically, T cells are collected from patients, manipulated *ex* vivo,

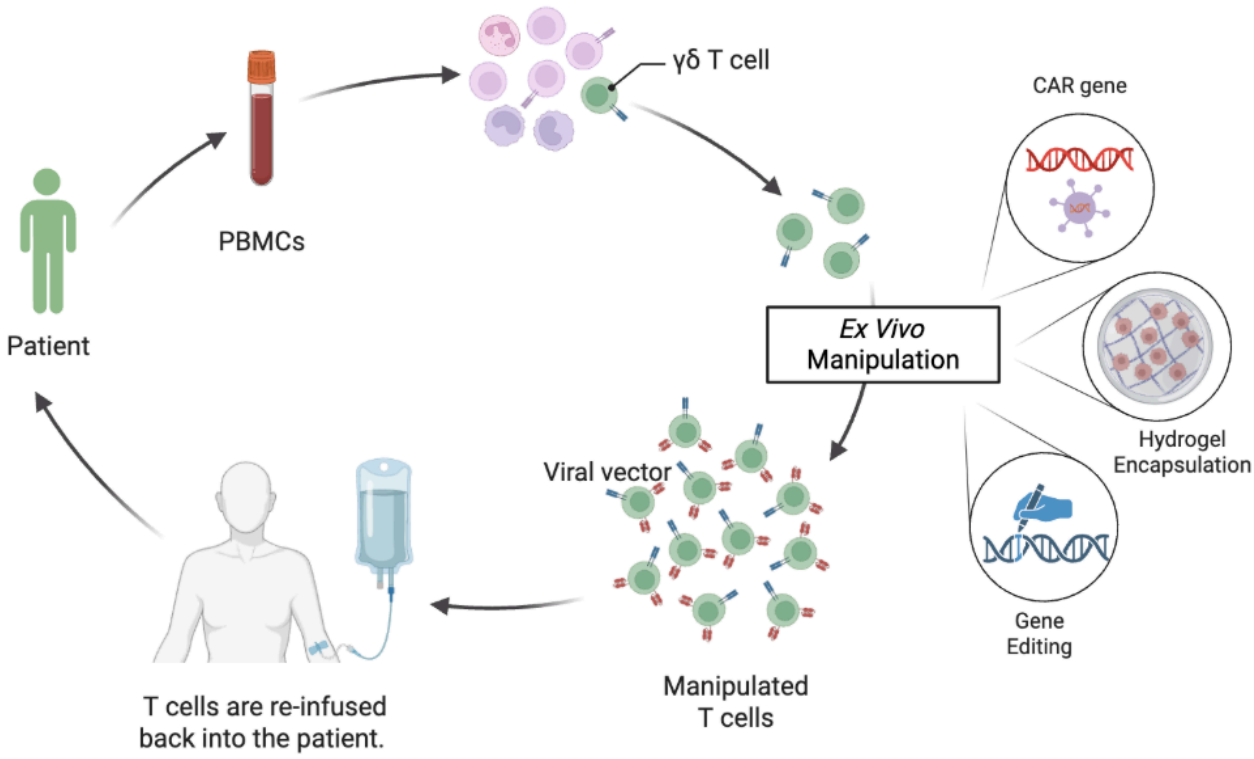

Figure 2. Schematic of γδ T-cell Adoptive Cell Therapy. PBMCs are collected from the patient and γδ T cells are isolated prior to ex vivo manipulation. During ex vivo processing, γδ T cells are modified via viral vectors, including CAR gene insertion and gene editing, or hydrogel encapsulation. Manipulated γδ T cells are subsequently reinfused into the patient for therapeutic application. Adapted from Biorender (2026). Original template available at Allogeneic Cancer Immunotherapy Using CAR γδ T Cells.

and re-injected back into the patient. Such manipulation includes the genetic modification of T cells to express novel or chimeric antigen receptors in order to overcome T cell exhaustion and circumvent immunosuppression. ACT therapies mark a new wave of personalized medicine that optimizes treatment for each patient in order to maximize effect and minimize toxicity (Morotti et al., 2021).

While ACT response rates are about 80% to 90% for hematological cancers, the response rate in solid cancer is only about 30% (Dougé et. al, 2024; Olson et. al 2023). This disparity reflects fundamental differences between hematological malignancies and solid tumors, which are characterized by dense extracellular matrices, abnormal vasculature, and immunosuppressive tumor microenvironments.

One major limitation is that physical barriers limit T cell infiltration into the TME. Within this hostile tumor microenvironment (TME), tumor associated macrophages (TAM) play a dominant role in limiting ACT efficacy. Specifically, TAMs promote the recruitment and immunosuppressive activity of Tregs, while simultaneously forming long-lasting physical bonds with $CD8^+$ T cells, impeding motility into the microenvironment (Xia et al., 2024; Peranzoni et al., 2018). Beyond restricting physical infiltration, tumor cells often downregulate the MHC I presentation pathway, causing them to be less detectable of $CD8^+$ T cells (Dhatchinamoorthy et al., 2021). Furthermore, since many cancer-associated antigens are also expressed on healthy cells, the dosage of ACT is limited in order to prevent off-target effects and cytokine release syndrome (Escobar et al., 2018).

Because the majority of ACT therapies utilize $\alpha\beta$ T cells, which require intact MHC-mediated antigen presentation, these combined physical and molecular barriers enable

many solid tumors to escape the immune system, weakening the overall efficacy of ACT therapies.

2.3 Gamma Delta ($\gamma\delta$) T cells

Comprising of 0.5-16% of all T lymphocytes, $\gamma\delta$ T cells remain to be the smallest subset of T lymphocytes (Deseke et al., 2020). Similar to $\alpha\beta$ T cells, $\gamma\delta$ T cells mature in the thymus from progenitor T cells, which originate from hematopoietic stem cells. However, rather than expressing pre-TCR during the developmental phase, $\gamma\delta$ T cells express TCR-$\gamma\delta$, committing to

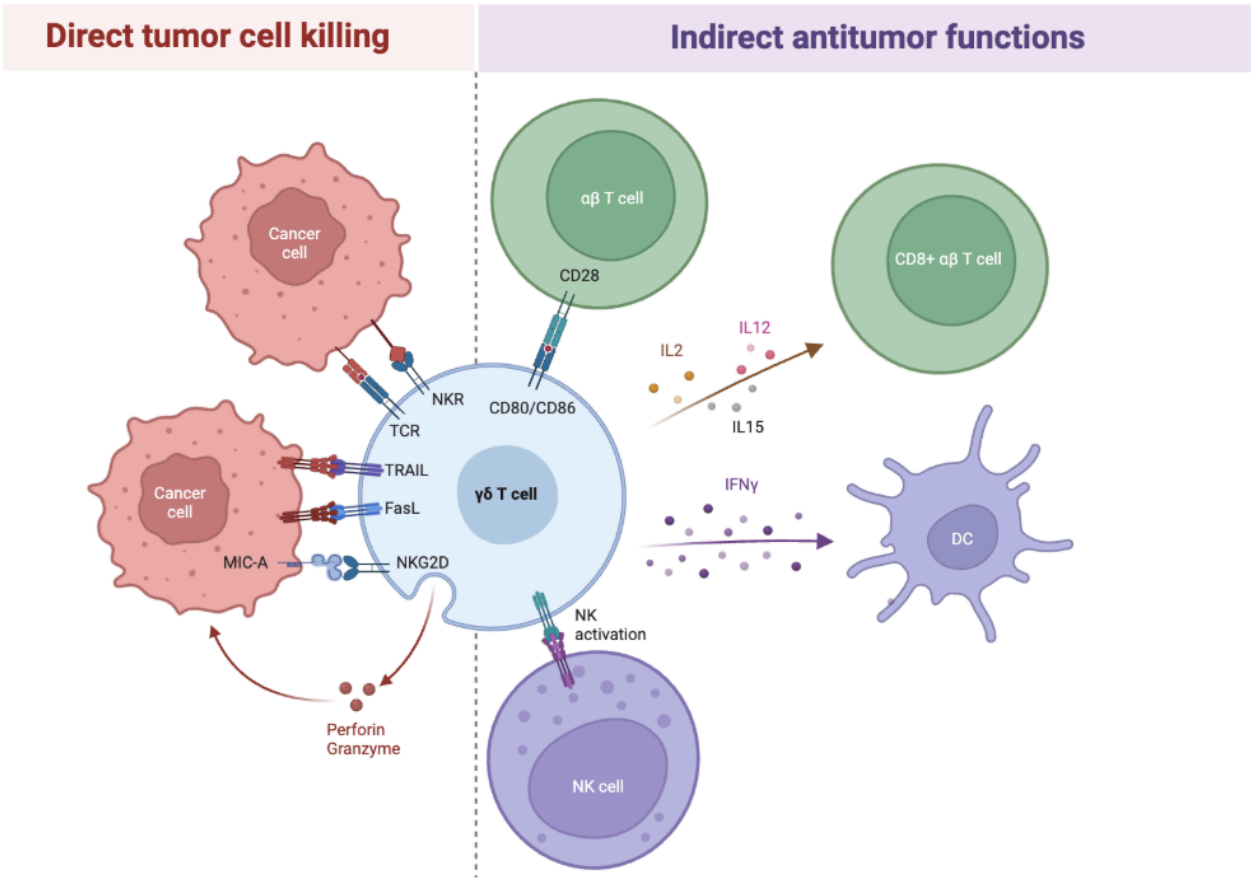

Figure 3. Schematic of γδ T cell-mediated antitumor responses. The figure illustrates the direct tumor cell killing by γδ T cells through the interaction of various surface markers (e.g., NKR, FasL, TRAIL) and the release of perforin and granzymes, as well as indirect antitumor functions via γδ T cell interactions with CD8+ αβ T cells, NK cells, and dendritic cells (DCs). This includes the activation of immune responses through cytokines like IFNγ, IL2, IL12, and IL15.Adapted from Biorender (2026). Original template available at Antitumor Activity of γδ T Cells.

a separate lineage. This difference in commitment is dependent on Notch signaling and TCR signal strength. While αβ T cells undergo stages of double-negative, double-positive, and single-positive during development, γδ T cells exit the thymus during the double-negative phase. This eliminates the requirement for co-receptor activation through MHC, class I, allowing γδ T cells to recognize a broader range of antigens (Hayday et al., 2009).

Characterized by their unique TCR composed of a γ and δ chain, gamma delta T cells (γδ) bridge the gap between innate and adaptive immunity. Innate immunity is the body's immediate, non-specific reaction to detect and eliminate pathogens, while adaptive immunity is the specialized, slower defense system that includes the development of long-lasting memory cells. The distinctness of γδ T cells lies in their unconventional ability to recognize antigens through tissue stressors, generally referred to as "lymphoid-stress surveillance" (Hayday et al., 2009). This allows for the circumvention of the MHC complex, a crucial recognition mechanism for αβ T cells. Since γδ T cells do not require MHC complex presentation for cell recognition, instead recognize and attack cancer cells by interacting with stress markers, phosphoantigens, and innate signals by NK killer cells and dendritic cells (Dong et al., 2022).

In terms of innate immunity, MHC independence allows for rapid production and release of cytotoxic cytokines, partially attributing γδ T cells to the first line of defense. Specifically, γδ T cells express a variety of innate-like receptors, such as toll-like receptors (TLRs), natural killer receptors (NKR), scavenger receptors, and lectin receptors, to interact with stress-induced MHC Class I Chain A (MIC-A), MHC Class I Chain B (MIC-B), and UL-166 Binding Proteins (ULBPs) (Hedges et al., 2020; Poggi & Zocchi et al., 2014). γδ T cells can also recognize tumor-associated antigens and phosphoantigens produced by cancer cells through antibody-dependent cell-mediated cytotoxicity. They can directly initiate apoptosis through the

perforin-granzyme mechanism, Fas/FasL, and TRAIL pathways, and stimulate an immune response by secreting anti-tumor cytokines like interferon-γ (IFN-γ), tumor necrosis factor-α (TNF-α), interleukin (IL)-2 , IL-10, IL-12, and IL-15 (Luo et al., 2024).

In terms of adaptive immunity, $\gamma\delta$ T cells have the ability to recruit dendritic cells and act as antigen-presenting cells (APCs) for $\alpha\beta$ T cells (Kabelitz et al., 2011). Activated $\gamma\delta$ T cells express high levels of MHC Class II and the CD28 ligands, CD80 and CD86, indicating antigen presenting functionality. Moreover, they can uptake and cross-present microbial and tumor-associated antigens through MHC class I and II to promote a CD8+ T cell response (Moser et al., 2006). Studies have also shown that $\gamma\delta$ T cells can develop immune memory similar to $\alpha\beta$ T cells, resulting in recognition of specific antigens and upon re-exposure, mount a faster and stronger immune response (Davey et al., 2018). As a result, these unique characteristics and versatility of $\gamma\delta$ T cells makes them a promising alternative strategy for adoptive cell therapy (ACT) in treating solid cancers.

2.3 Current Clinical Landscape of Gamma Delta T cells

While most adoptive immunotherapies have focused on αβ T cells, novel therapies using γδ T cells have shown limited success. Specifically, γδ T cell therapies have predominantly been effective in hematological malignancies. One possible reason for this limitation is that the majority of these therapies rely on Vδ2 γδ T cells, a blood-based subset that is easier to obtain, however, lacks the ability to penetrate and reside in tissues. As a result, a significant limitation of these therapies is the lack of cell infiltration into the solid tumor microenvironment.

Currently, there are four subsets of immunotherapies: autologous transfers, allogenic transfers, stimulation of *in vivo* γδ T cells via cytokines, and CAR γδ T cell therapies.

Autologous and allogenic transfers both involve the transfer of cells into a patient's body, however, autologous transfers utilize cells directly from the patient, while allogenic transfers are cells derived from donors. In addition, some therapies aim to stimulate in vivo γδ T cells with stimulators and/or the administration of γδ T cells as co-treatments with adjunct therapies (Nicol et al., 2011). Chimeric Antigen Receptor (CAR) γδ T cell therapy is a personalized immunotherapy that genetically alters γδ T cells for enhanced ability to recognize and kill cancer cells.

Currently, allogeneic treatment using γδ T cells from health donors have proven to be clinically safe and more effective in the treatment of solid tumors than autologous transfers. This

Table 1: Overview of current γδ T cell immunotherapy strategies and their limitations.

Therapy Type	Description	Advantages	Key Limitations
Autologous Transfers	γδ T cells isolated from the patient, expanded ex vivo, and reinfused	Avoids immune rejection	Limited cell numbers, poor tumor infiltration
Allogenic Transfers	δ T cells obtained from healthy donors and transferred to patients	Potential graft-vs-tumor effect; scalable cell sources	Spatial localization issues; cells migrate to lungs, liver, spleen
In Vivo Stimulation	Activation of endogenous γδ T cells using cytokines or chemokines	Non-invasive; activates patient's immune cells	Nonspecific activation; risk of autoimmune responses
CAR γδ T cells	Genetically engineered γδ T cells expressing chimeric antigen receptors	Improved tumor recognition and cytotoxicity	Poor trafficking to tumors; cytokine release syndrome

may be due to the graft-vs-tumor effect, in which the donor's cells can recognize and kill cancer cells (Revesz et al., 2024). However, one major obstacle is cellular spatial localization. For example, a 2011 phase I clinical trial showed that adoptively transferred γδ T cells typically migrated to the lungs, liver, and spleen, while the remaining portion was found in the metastatic tumor site (Nicol et. al, 2011). Other attempts to better spatially program γδ T cells include in vivo stimulation through cytokines and chemokines. While studies did find that this reduced local metastasis, some patients experienced new metastases at distant sites. Furthermore, attempts at stimulating γδ T cell surface markers to enhance T cell efficacy is that this stimulation is nonspecific and could lead to autoimmune issues (Cieslak et al., 2025). The use of CAR γδ T cells have been at the frontline of contemporary immunotherapies. However, similar to autologous and allogenic transfers, poor results continue to stem from poor trafficking of cells into tumors. Moreover, the aggressive nature of the immune response generated from γδ T cells have led to cytokine release syndrome, a systemic inflammatory response caused by an overreactive immune system (Murad et al., 2025).

Overall, current γδ T cell–based immunotherapies remain limited by poor spatial localization and inefficient infiltration into solid tumors. Approaches such as adoptive transfer, in vivo stimulation, and CAR engineering have each demonstrated partial success, yet none have fully overcome the physical and biochemical barriers imposed by the solid tumor microenvironment. This thesis investigates an alternate strategy in increasing infiltration into tumors through hydrogels encapsulation to promote a tissue residency phenotype. Addressing these spatial and mechanical constraints may be critical for unlocking the full therapeutic potential of γδ T cells in solid cancer treatment.

2.4 Collagen as a Biomaterial

Collagen is a ubiquitous fibrous protein that constitutes the majority of the extracellular matrix (ECM) in all animals and primarily maintains the structural integrity of tissues and organs (Rezvani et al., 2021). To date, there are 28 types of collagen. Type I, II, III, and V are the main types that make up the essential part of collagen in bond, cartilage, tendon, skin, and muscle (Cen et al., 2008). Furthermore, collagen as part of the extracellular matrix naturally can promote cell adhesion, migration, proliferation, differentiation, and play a critical role in cell-to-matrix

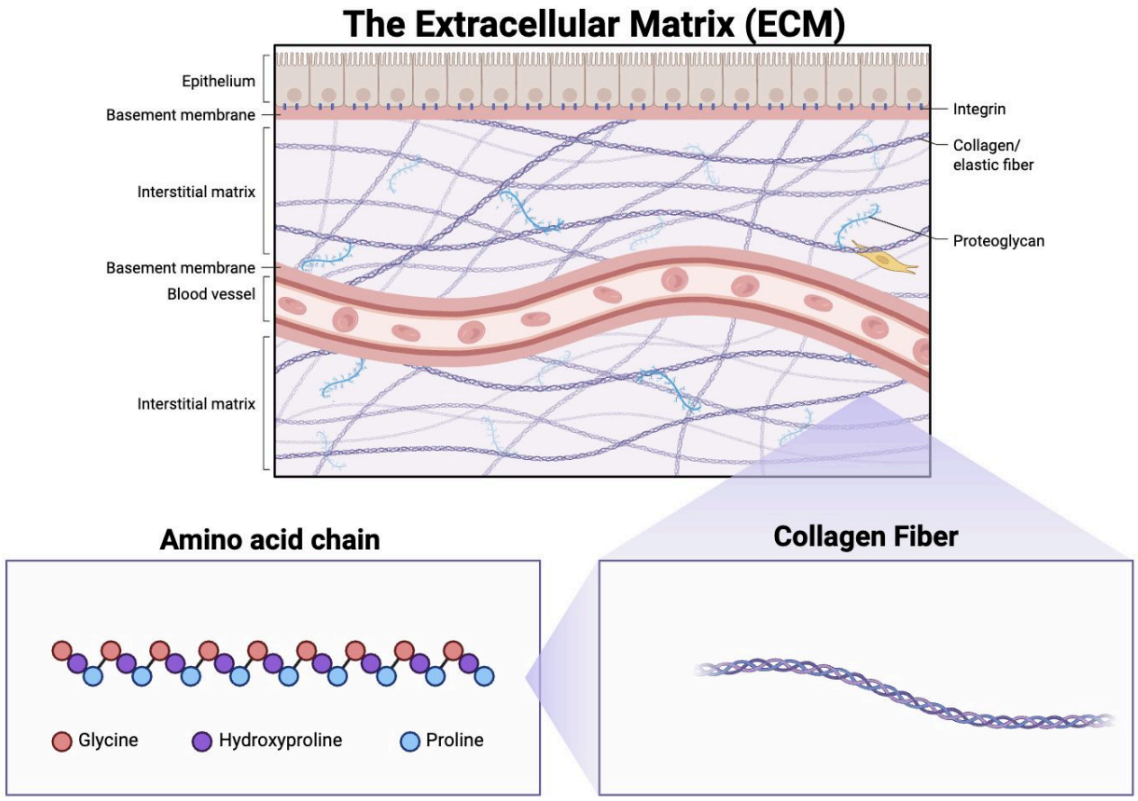

Figure 4. Schematic of collagen and its role in the ECM. Collagen fibers are distributed throughout the interstitial matrix and basement membrane, where they provide mechanical support and transmit forces between cells and their surrounding environment. At the molecular level, collagen is composed of amino acid chains enriched in a repeating glycine–proline–hydroxyproline sequence. Made from Biorender (2026).

interaction (He et al., 2025). In addition, collagen as a biomaterial can enable nutrients to travel and be exchanged more easily due to its high porosity and hydrophilicity, ensuring that cell life and function can be maintained (Thirumalaivasan et al., 2025). Due to collagen's excellent biocompatibility, biodegradability, flexibility, and mechanical strength, it is a highly versatile biomaterial that has been used for wound healing, gene delivery carriers, and injectable systems (Khan et al., 2013).

The structure of collagen is three alpha (α) protein chains that are wound together to form a triple helix. Each alpha chain is composed of a repeating sequence of three, where a glycine residue is in every third system. Since glycine is the smallest amino acid, it brings together the three helical α chains. The two other amino acids are often proline and hydroxyproline (Zhu et al., 2022). Furthermore, the individual triple helices can be arranged to form fibrils that are of high tensile strength and can be further cross-linked to support stress more efficiently (Khan et al., 2013).

2.5 Mechanical Influences on T cell Phenotypes

Mechanical properties of the cellular microenvironment are increasingly recognized as important regulators of immune cell behavior**.** During an immune response, tissues such as lymph nodes undergo dynamic mechanical changes, transiently stiffening as immune cells become activated before returning to a softer baseline state (Meng et al., 2020). These observations suggest that immune cell activation, differentiation, and function are closely linked to the mechanical context in which cells reside.

Emerging studies show that T cell phenotypes are affected by the mechanical properties of their anatomical locations. For example, immune cells have mechanosensitive ion channels

that can convert external mechanical forces into electrical and chemical signals. This signaling pathway can regulate the inflammatory response in immune cells (Xia et al., 2024). Furthermore, certain receptors on the cell membrane of immune cells are mechanosensitive. One example is PD1 expression, a common immune checkpoint receptor and marker for T cell exhaustion that is known to be mechanosensitive. Specifically, PD1-PDL1 ligand bonding can regulate actin rearrangement and lamellipodia formation, suggesting that PD1 is mechanosensitive (Li et al., 2024).

Currently, there is a growing body of biomechanical studies that aims to elucidate how the physical properties of the cellular microenvironment regulate immune cell behavior. In particular, it has been demonstrated that functionally distinct populations of αβ T cells can be generated through precise tuning of the mechanical properties of tissue-mimetic hydrogels via the activator-protein-1 signaling pathway, which is a critical regulator in T cell activation and fate (Adu-Berchie 2023). Building on these findings, this thesis aims to investigate whether similar mechanical regulation can be extended to γδ T cells.

2.6 The Morphology of γδ T cell Migration

Athough γδ T cells have been increasingly studied for their roles in immune surveillance and tissue immunity, relatively little is known about the mechanisms governing how they migrate through extracellular matrices. Most insights into T cell migration instead come from studying αβ T cells. In three-dimensional collagen matrices, αβ T cells typically exhibit amoeboid-like migration, characterized by rapid, non-adhesive movement through the matrix. During this process, cells crawl along collagen fibrils through contact guidance, using the alignment of fibers to help direct their movement (Wolf et al., 2003). In general, there are two physical factors that

strongly influence migration efficiency. The first is the porosity of the ECM, which determines whether sufficiently large gaps exist for cells to pass through. The second is the cell's ability to deform its nucleus to squeeze through fibers in the ECM (Fischer et al., 2020) . While many studies have examined the tissue locations where γδ T cells migrate, there is not much knowledge on the morphological characteristics of their movement. Consequently, it remains unclear whether γδ T cells rely on similar amoeboid strategies as αβ T cells or whether they display distinct migratory behaviors in three-dimensional matrices. While this paper is primarily focused on the migrational speeds and the tissue-resident phenotypes, the confocal imaging could help uncover some insight on the morphological behavior of T cell migration.

2.6 Mechanosensitive Pathways and Tissue-Resident Markers

In this study, we stained γδ T cells for programmed cell death protein 1 (PD-1), DNAX accessory molecule-1 (DNAM-1/CD226), Natural Killer Group 2 member D (NKG2D), and cluster of differentiation 11a (CD11a) to characterize their tissue-adapted state. These receptors are characteristic of tissue-resident and tissue-sensing lymphocytes and were used to identify this population.

Specifically, it has been shown that PD-1 expression on γδ T cells marks a distinct, tissue-adapted functional state rather than a T cell exhaustion phenotype for αβ T cells (Davies et al., 2024). Furthermore, γδ T cells express DNAM-1, which binds CD155 and CD112 on tissue or tumor cells, thereby enhancing target recognition and promoting activation (Jianzhen et al., 2025). NKG2D, a common natural killer cell receptor, functions as a stress and "tissue status" sensor by recognizing ligands that are upregulated on stressed, infected, or transformed cells within peripheral tissues (Hayday et al., 2019). CD11a, which is expressed by most γδ T cells, is

a key component of lymphocyte function–associated antigen-1 (LFA-1) and mediates adhesion to endothelial and other cells, supporting tissue retention and trafficking (Siegers 2018). As a result, this paper aims to uncover how the expression of PD-1, DNAM-1, NKG2D, and CD11a can be altered through changes in the mechanical properties of the hydrogels.

Chapter Three: Materials and Methods

3.1 Materials Preparation

Rat Tail Collagen Type I (Gibco 17104019) was functionalized with-norbornene-2-acetic acid succinimidyl ester (Nb-NHS) at a ratio of 0.1 g Nb-NHS:1 g collagen. Nb-NHS was dissolved in dimethyl sulfoxide (DMSO) to an initial concentration of 2mg/ml and diluted 10-fold in 1xPBS. This solution is then added to the neutralized collagen by NaOH. This reaction proceeded for 5 hours at 4 °C under rigorous stirring to delay collagen gelation. 0.1 N acetic acid was added to quench the reaction and re-acidify the collagen solution. Norbornene-modified collagen (Col-NB) was dialysed in 0.025 N acetic acid for 4 days. It was then filtered with a 0.45 µm filter and then lyophilized for future use.

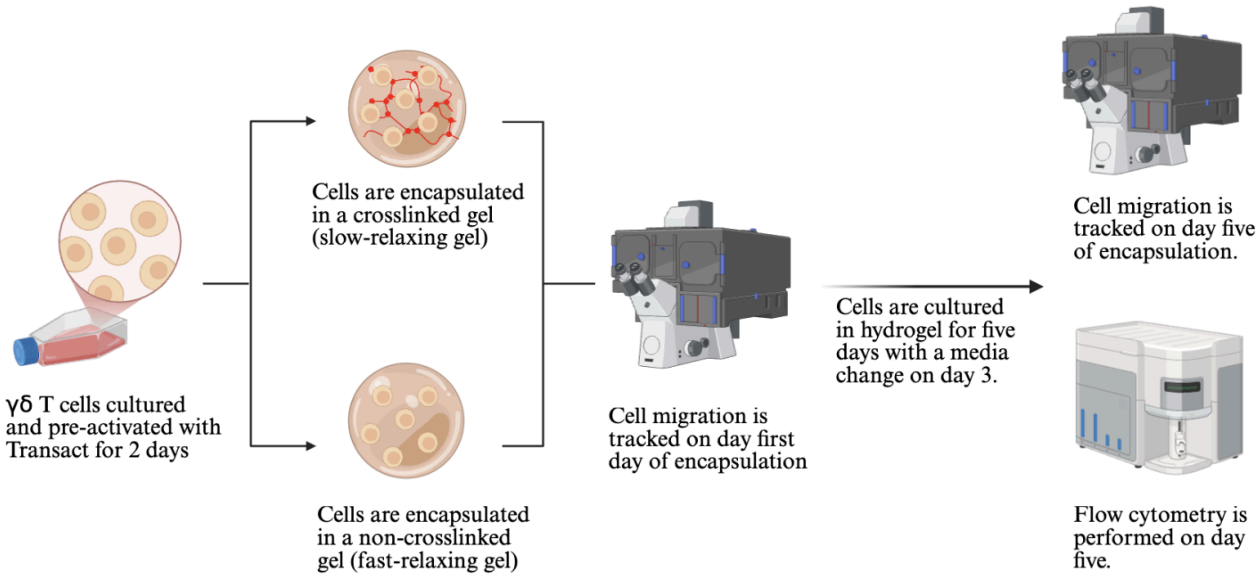

Figure 5. Experimental setup for overall γδ T-cell encapsulation, migration tracking, and flow cytometry.

3.2 Gel Synthesis and Col-Nb cross-linking

Lyophilised Col-Nb is dissolved to 9 mg ml^{-1} in 0.025 N acetic acid at 4 °C overnight. Prior to collagen solution preparation, all reagents including the 48 well MatTek plates are placed on ice to avoid premature gelation. Prior to casting the gel, the pH of the final gel was tested on pH strips. The final pH is between 7-7.5 and a final collagen concentration to 2 mg ml^{-1}. The collagen solution must be neutral or close to neutral to avoid cell death when adding cells and to guarantee gelation. After gelation, the gel was submerged in MeTz-(PEG)5-MeTz crosslinker solution at different concentrations to allow diffusion to happen at 23 °C for 20 min. The cross-linking solution was then removed and the gel was incubated at 37 °C for one hour to allow for the click reaction to occur. If needed, rheological characterization was subsequently performed.

3.3 Rheology Characterization

Rheology characterization of the collagen-norbornene gels were performed on a stress-controlled, combined motor and transducer rheometer (AR-G2, TA instrument) with a 40 mm cone geometry. The collagen solution was made following the method described in section 3.2, and directly loaded onto the 37 °C heated plate on the rheometer. Two tests were performed. The first test, oscillatory time sweep, was conducted at at 37 °C for 10 min to measure the storage modulus (G′), loss modulus (G″), and the loss angle (δ, delta) at a frequency of 1 Hz and 1% strain. The shear stress relaxation test was performed by applying 10% strain within 1s and maintaining 10% strain while recording changes in shear stress for 0.5-2h at 37 °C. A humidity chamber and Kimtech wipes that were wetted with water were used to prevent gel dehydration during incubation.

3.4 T cell Isolation and Culture

Human PBMCs were obtained from Brigham and Women's Hospital and isolated from blood through a Ficoll gradient. $\gamma\delta$ T cells were isolated from PBMCs using the magnetic-bead-based TCR g/d+ T cell Isolation kit (Miltenyi Biotec), following the manufacturer's protocol. $\gamma\delta$ T cells were then activated with T cell Transact (Miltenyi Bitoec 5210705271) for two days. They were cultured in T cell media (RPMI, 10% heat inactivated fetal bovine serum, 1 % penicillin/streptomycin, 1% 100 nM sodium pyruvate (Gibco 2993916), 1% 100x nonessential amino acids (Gibco 2939008), 1M HEPES Buffer (Gibco 2986075), and 55 μM beta-mercaptoethanol. The media was also supplemented with recombinant human IL18 and IL15.

3.5 T cell Encapsulation

Transact-activated $\gamma\delta$ T cells were resuspended and washed twice in MACS Buffer. MACS Buffer is made from 1X Dulbecco's Phosphate Buffered Saline (Gibco, Bovine Serum Albumin 14190-144), (Sigma-Aldrich A1470-100G), and 0.5 M EDTA, pH 8.0 (Invitrogen AM9261). $\gamma\delta$ T cell viability and counts were determined through the Cytek Muse Cell Analyzer before being resuspended in PBS and added to the collagen solution at a final cell density of 25,000 cells per 50 microliters of collagen solution. This collagen solution was casted into a 48 well MatTek plate and follows the remaining methodology described in section 3.2. After collagen gelation, cross-linking, and incubation, collagen hydrogels underwent two 30 minute washes with T cell media supplemented by IL18 and IL15 to remove excess crosslinker. SIR-DNA was then added to the T cell media to stain all live cells for imaging for one hour. For plates that did not require SIR-DNA, hydrogels were still incubated for one hour in medium.

3.6 Flow Cytometry

To examine changes in phenotypic expression, all donors will be characterized using flow cytometry for the markers anti-human CD3 (BD Biosciences 570237), Anti-hu PE Vδ1 (Invitrogen 12-5679-42), APC anti-human Vδ2 (Biolegend 331418), anti-human PD1 (Biolegend 367426), Anti-Hu NKG2D (Invitrogen 25-5878-42), anti-human DNAM1 (Biolegend 338322), and CD11a (Invitrogen 11-0119-42). γδ T cells will first be removed by breaking up the collagen mechanically and with Collagenase Type IV. Cells will then be washed twice with MACs buffer to remove excess debris and dye and seeded in a 96-well U-bottom plate. All cells except for the no stain will be stained with Live-Dead Stain (Invitrogen L3224). After 20 minutes at room temperature, 100 microliters of FACS buffer will be added and centrifuged at 550 rcf for 3 minutes. Human TruStain FC Block (Biolegend 422302) will be added to prevent nonspecific binding for 15 minutes at room temperature and then stained with the flow fluorophores at 37 °C for 30 minutes. Staining will then be stopped by washing twice in FACs. To fix the plate, 16% paraformaldehyde (Electron Microscopy Sciences, EM Grade 15710-S) will be diluted to % by PBS and 100 microliters of this solution will be added to each cell. The plate will be kept at 4 °C for 10 minutes, while covered with foil, before being rinsed twice and resuspended in 200 microliters of PBS.

3.7 Confocal Microscopy

Confocal microscopy imaging of the Col-nb gels with cells were performed on a temperature and CO_2 controlled microscope (STELLARIS Leica). Images were scanned in two dimensions along the y and x axis at different z levels using a bidirectional laser. We used Alexafluor 647 and for cells stained with SIR-DNA (Cytoskeleton CY-SC007). Tiles and z levels were selected based on

the highest observed cell density. The total number of tiles selected per time point was twenty-four and each tile was imaged through 180 cycles. Cells were imaged for 6 hours and 30 minutes in 2 minutes and 18 second intervals, which was the minimum time needed to complete the 180 cycles of 24 tiles.

3.8 ImageJ Analysis

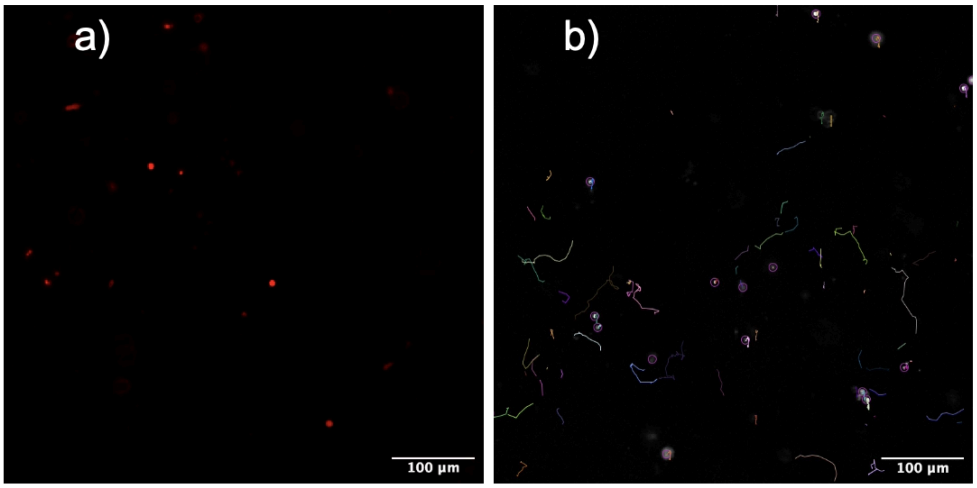

Figure 6. Cell Tracking Using ImageJ. a) Cells were initially labeled with SiR-DNA, a nuclear dye that stains DNA and enables clear visualization of individual cells within the 3D matrix b) Time-lapse image sequences were then analyzed using the TrackMate plugin in ImageJ, which identifies cells and reconstructs their migration trajectories. Note: Subsequent analysis demonstrated that cell trajectories could be reliably generated using TrackMate detection parameters alone, indicating that nuclear staining was not required for effective tracking of γδ T-cell movement in this system.

The migratory analysis was performed by Trackmate, a detector interface distributed by Fiji (Ershov et al., 2022). Specifically, we utilized this detector to apply a LoG(Laplacian of Gaussian) filter to the images in either SIR-DNA or FITC dye channel. The calculations were made in the Fourier space. The local maximums in the filtered image are searched for, and maximums that are too close are suppressed, creating an almost binary image that allows for subpixel localization. We selected that our cell would be roughly 10 microns in diameter. We selected the linking maximum distance to be 15 microns and a gap-closing max frame gap.

Trackmate helped calculate the distance traveled between each frame for each cell, which is marked as a “spot”. We used Python to calculate the mean squared displacement (MSD) and the average speed. Only cells moving for ten or more frames were incorporated into this study.

3.9 Statistical Analysis

Basic statistics, including the mean and standard deviation, were calculated using Microsoft Excel. Statistical analyses were performed in Python within the Jupyter Notebook. Differences between slow-relaxing and fast-relaxing hydrogels were evaluated using paired t-tests. Statistical significance was defined as $p < 0.05$. All bar graphs and visualizations were generated using Python in the Jupyter Notebook. All code utilized for this thesis is included in the appendix.

Chapter Four: Development and Characterization of a Tunable Collagen Hydrogel System

4.1 Synthesizing a collagen hydrogel-based ECM with tunable viscoelastic properties

A collagen-type-I-based ECM model was utilized to tune matrix stiffness and viscoelasticity (Figure 7a). Stiffness refers to an object's resistance to deformation, while viscoelasticity refers to a material's time-dependent response to stress. Type 1 collagen was used as it is the most abundant protein found in vertebrates and essential in maintaining chemical and structural integrity (Li et al., 2024). Collagen type I was first modified with norbornene, which undergoes an inverse electron demand Diels-Alder (iEDDA) click reaction with the crosslinker, methyltetrazine (Adu-Berchie et al., 2023).

Matrix stiffness is dependent on collagen concentration, while viscoelasticity is dependent on the concentration of cross linker used. Mechanical characterization showed that stiffness and viscoelasticity could be tuned independently of one another. Specifically, an increase in collagen concentration solely tuned hydrogel stiffness (Figure 7b, 7c), while crosslinker addition only tuned shear stress relaxation (Figure 7d, 7e). Increasing crosslinking of a gel leads to a more elastic gel, while no crosslinking leads to a more viscoelastic gel. The stiffness of the gel was calculated utilizing the Young's modulus equation, where Young's modulus (E) is equal to 2G'(1+V). G' is the shear or storage modulus in viscoelastic materials, while V is Poisson's ratio. The Poisson's ratio for our biomaterial is 0.5. Collagen modification and cross linkers have little effect on T cell phenotype (Adu-Berchie et al., 2023).

A collagen concentration of 2 mg/mL and a crosslinker concentration 316 μm was selected for subsequent studies. This concentration most closely approximates the mechanical

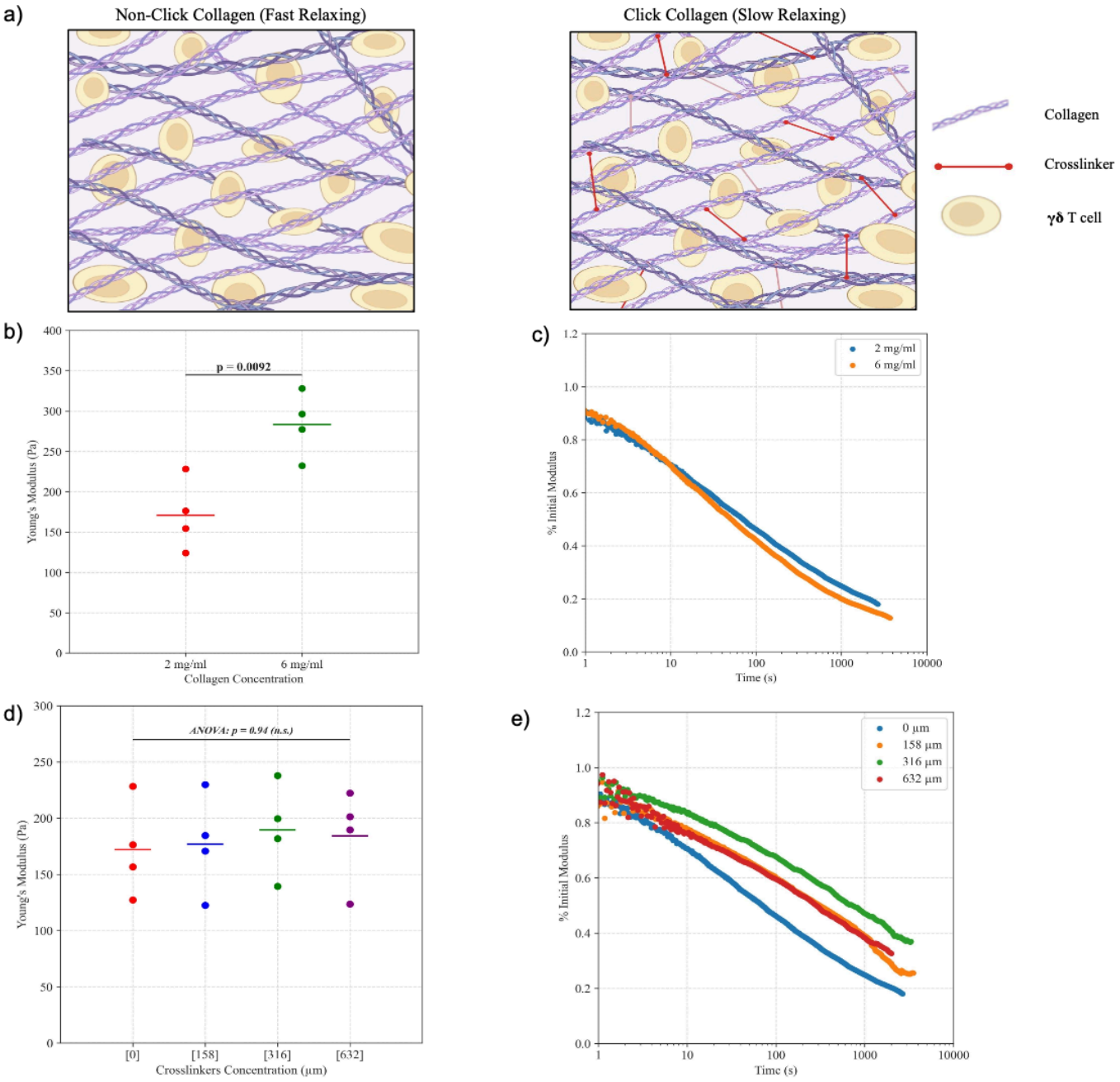

Figure 7: Synthesizing tissue mimetic collagen hydrogels with tunable mechanical properties. a) Schematic of collagen hydrogel showing non-click collagen (fast-relaxing) and click collagen (slow-relaxing) b) Young's moduli under constant deformation for varying collagen concentration c) Changes in hydrogel stiffness is independent from viscoelastic properties as shown by the shear stress deformation as shown by percentage of initial modulus d) Changes in viscoelastic properties is independent from stiffness. e) Shear stress deformation of varying cross linker concentration as shown by the percent modulus

properties of the native lymph node extracellular matrix, which regulates immune cell migration stiffness of the lymph node. Prior studies have shown that lymph node tissue typically exhibits elastic moduli in the low kilopascal range, similar to those observed in collagen hydrogels at approximately 2 mg/mL (Adu-Berchie et al., 2023) .

4.2 Hydrogel Encapsulation

γδ T cells cultured on 2D substrates display increased clustering and aggregation, while cells encapsulated in the slow- and fast-relaxing matrix appear more evenly distributed. γδ -cells were all seeded at a density of 5 x 10^5 cells per milliliter of hydrogel. Furthermore, in Figure 8b and 8c, it can be observed that cells are suspended throughout the three-dimensional matrix rather than being confined to a single plane. This is evident from the variation in focus across the field and confirms successful encapsulation of γδ T cells within the 3D collagen hydrogel environment. No clear qualitative morphological differences are visible between the slow- and fast-relaxing hydrogels.

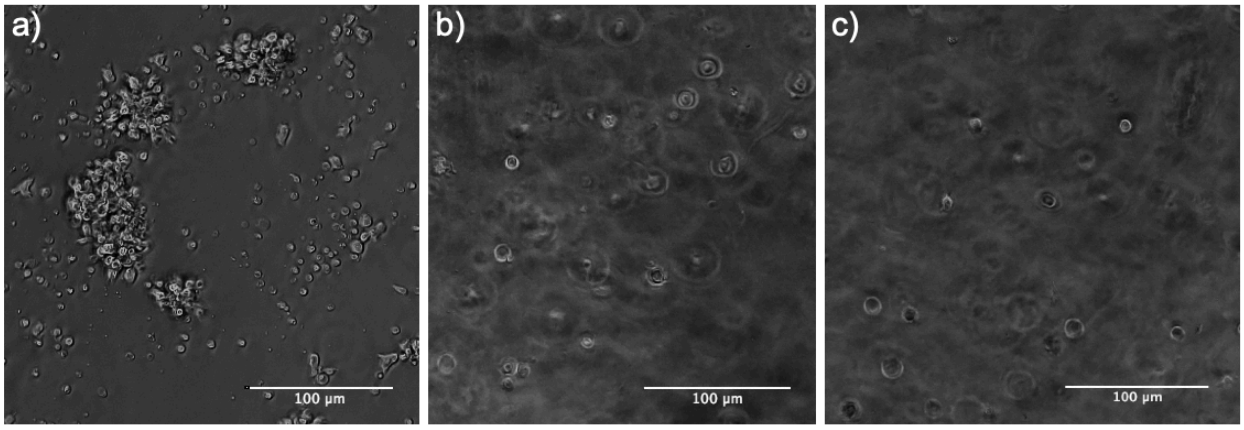

Figure 8. Matrix viscoelasticity alters γδ T cell spatial organization in collagen hydrogels. Representative brightfield images of γδ T cells cultured under different matrix mechanical conditions. a) 2D culture control b) slow-relaxing hydrogel c) fast-relaxing hydrogel.

Chapter Five: Results

5.1 The Morphology of γδ T cell Migration

γδ T cells elongate and probe their environment as they migrate, exhibiting an amoeba-like mode of movement, rather than maintaining their circular shape. They glide across surfaces by continuously extending and retracting membrane protrusions in multiple directions, which allows them to wander and migrate throughout the hydrogel. This movement may reflect active actin remodeling, which enables surface probing and navigation; however, further imaging with actin staining would be needed to confirm this.

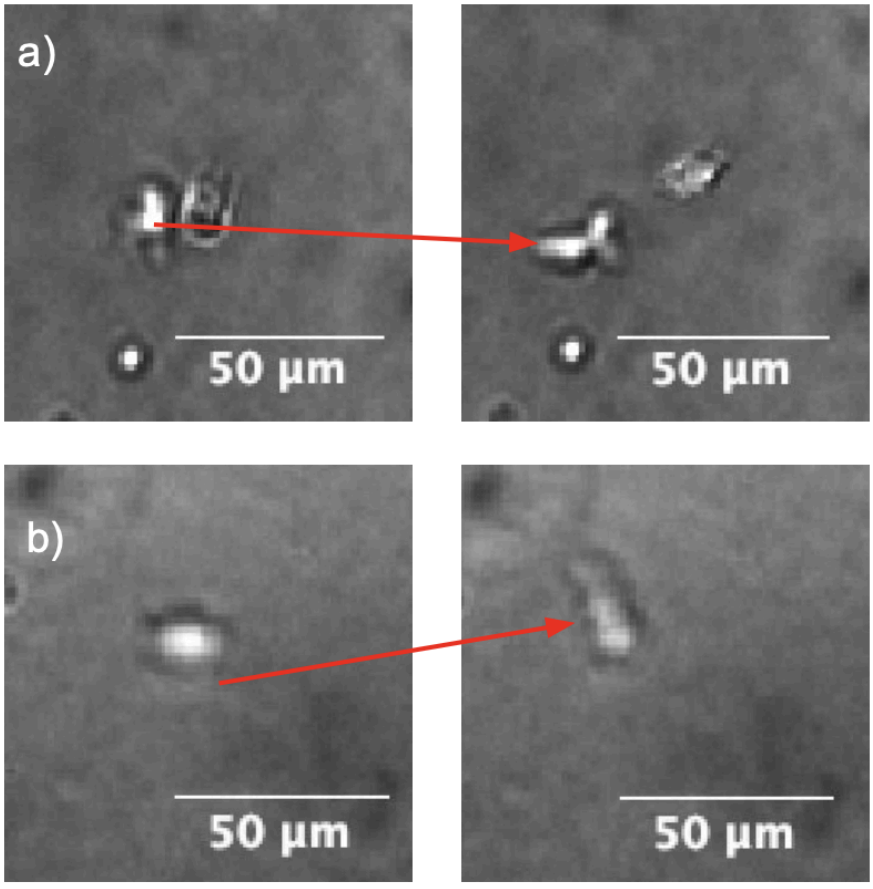

Figure 9. T cells elongate and probe the environment during migration. (a, b) Time-lapse images showing individual T cells that transition from a rounded to an elongated morphology as they move. In each panel, the red arrow corresponds to the same cell two frames later.

5.2 Fast-Relaxing Hydrogels Promotes Increased Cell Migration and Distribution by Day 5

Following encapsulation in the hydrogel matrices, γδ T cell migration was imaged on Day 0 and Day 5 to capture their overall migrational patterns. For each tracked cell, the starting position was normalized to the origin prior to plotting migration trajectories. Time-lapse imaging was performed over 180 frames at two-minute and 18 second intervals across 24 z-sections, corresponding to the time required to capture a full imaging cycle. A z-section refers to an optical slice taken at a specific depth within the hydrogel along the z-axis, allowing cells distributed throughout the three-dimensional matrix to be imaged. The total imaging duration was 6 hours and 54 minutes. Day 0 imaging began approximately four hours after initial gelation of the hydrogels.

In all three donors, it was observed that most γδ T cells on Day 0 remained within approximately 25 μm of their starting positions, regardless of whether they were encapsulated in a slow-relaxing or fast-relaxing hydrogel. However, by Day 5, cells in the fast-relaxing condition displayed substantially longer migration trajectories and extended up to 100 microns away from their points of origin. This increase in displacement suggests that cell motility is enhanced in fast-relaxing matrices over time. Furthermore, this could indicate that more viscoelastic environments could facilitate immune cell migration by allowing cells to more readily deform and remodel the surrounding extracellular matrix. Overall, the differences captured by imaging show that γδ T cells have the capability to mechanosense and adapt over time to the environments that they inhabit.

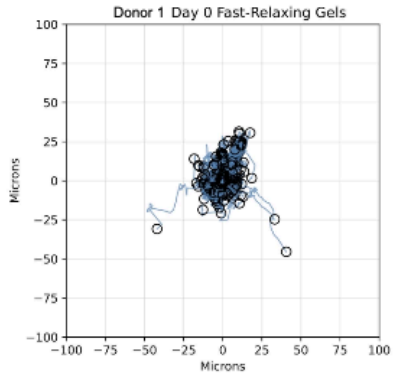
Donor 1 Day 0 Fast-Relaxing Gels
Microns
Microns

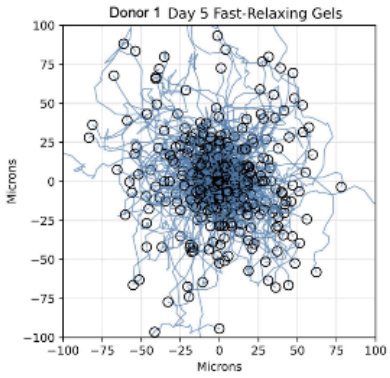
Donor 1 Day 5 Fast-Relaxing Gels
Microns
Microns

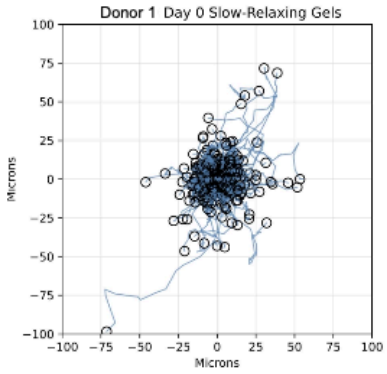
Donor 1 Day 0 Slow-Relaxing Gels
Microns
Microns

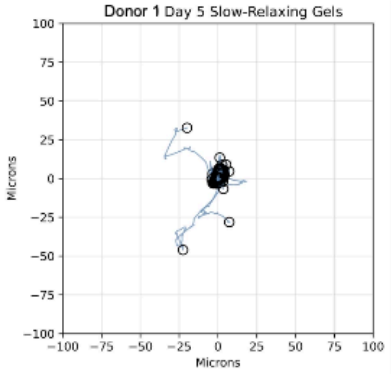
Donor 1 Day 5 Slow-Relaxing Gels
Microns
Microns

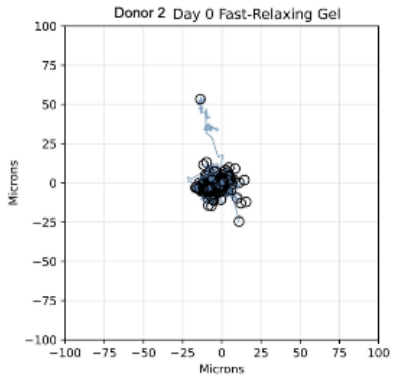
Donor 2 Day 0 Fast-Relaxing Gel
Microns
Microns

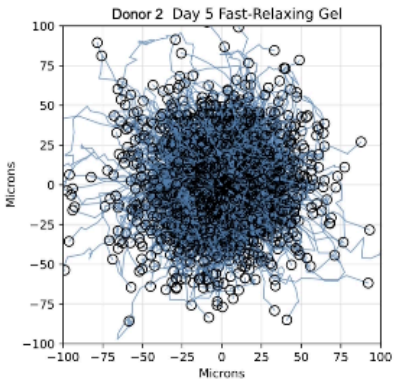
Donor 2 Day 5 Fast-Relaxing Gel
Microns
Microns

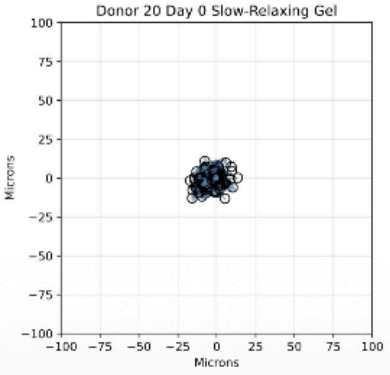
Donor 20 Day 0 Slow-Relaxing Gel
Microns
Microns

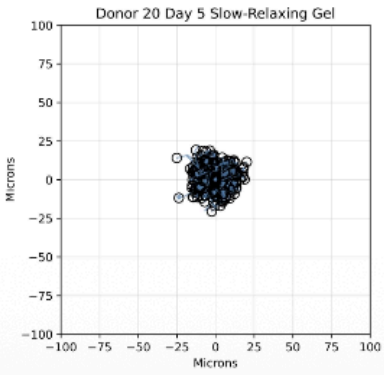
Donor 20 Day 5 Slow-Relaxing Gel
Microns
Microns

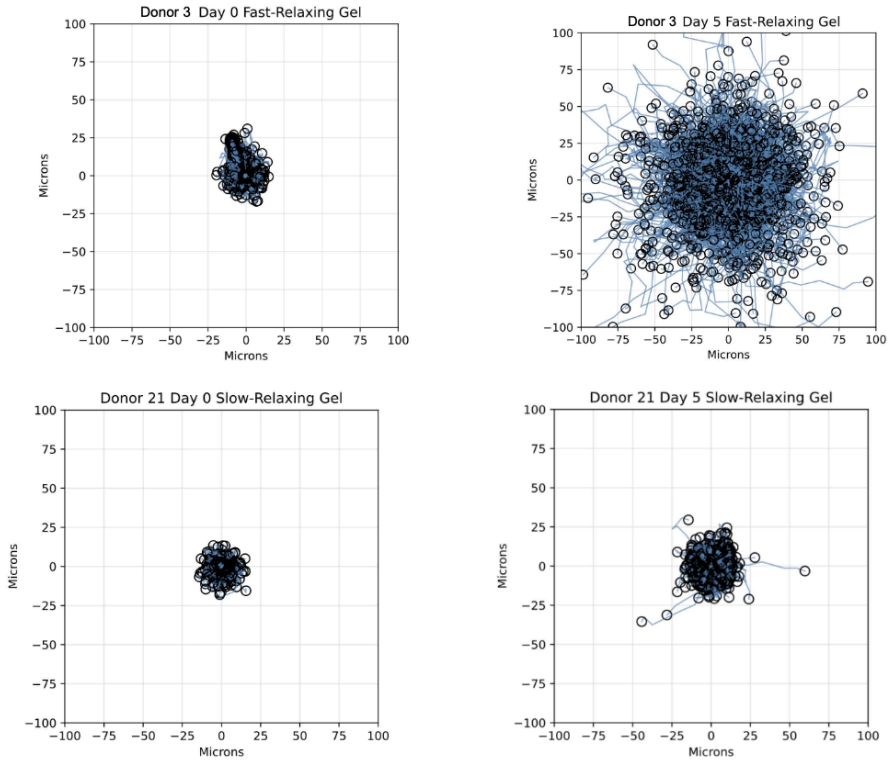

Figure 10: Fast-relaxing hydrogels promote increased γδ T cell migration over time. Migration trajectories of γδ T cells encapsulated in fast-relaxing collagen hydrogels for three donors on Day 0 and Day 5. Left Column (Day 0): Cells from all donors remain tightly clustered near the origin, indicating limited migration shortly after encapsulation. Right Column (Day 5): The trajectories for fast-relaxing gels extend substantially farther from the origin across all donors, demonstrating increased cell displacement and motility.

5.3 γδ T Cell Migration Remains Limited in Slow-Relaxing Hydrogels by Day 5

On the contrary, γδ T cells encapsulated within slow-relaxing collagen hydrogels remained highly localized around their initial positions on both Day 0 and Day 5. Across all three donors, the majority of cells remained within approximately 25 μm of their point of origin, forming dense clusters centered near the origin. Only a small number of cells displayed longer trajectories. In addition, comparing Day 0 and Day 5 conditions revealed that there was minimal overall expansion of migration trajectories over time. Even in Donor 1, where there was a small number of cells that possessed a displacement greater than 25 μm, the majority of trajectories

cluster near the origin with a reduction in the number of cells that exhibit a displacement greater than 25 μm by day 5. Across all donors, there are a small number of individual tracks that extend beyond 25 μm, however, the majority of cells continued to exhibit restricted movement even after several days within the matrix. This limited displacement suggests that the slow-relaxing hydrogel environment decreases γδ T cell motility, which may be aligned with tissue-residency and tissue localization.

5.4 Fast-Relaxing Hydrogels Promote Higher Migrational Speed and Mean Squared Displacement at Day 5

On Day 0, no statistically significant differences were observed between slow-relaxing and fast-relaxing hydrogels in either γδ T cell migrational speed or mean squared displacement. Across all three donors, average cell speeds on Day 0 were approximately 0.01 μm/s, while Mean squared displacement values remained below 20 μm^2, indicating minimal overall displacement from the initial position regardless of hydrogel relaxation properties. Mean Squared Displacement was calculated based on the average squared distance between a cell's starting location and its position at later time points. Because the displacement is squared and averaged across time intervals, MSD captures not only directional movement but also the extent of random wandering behavior.

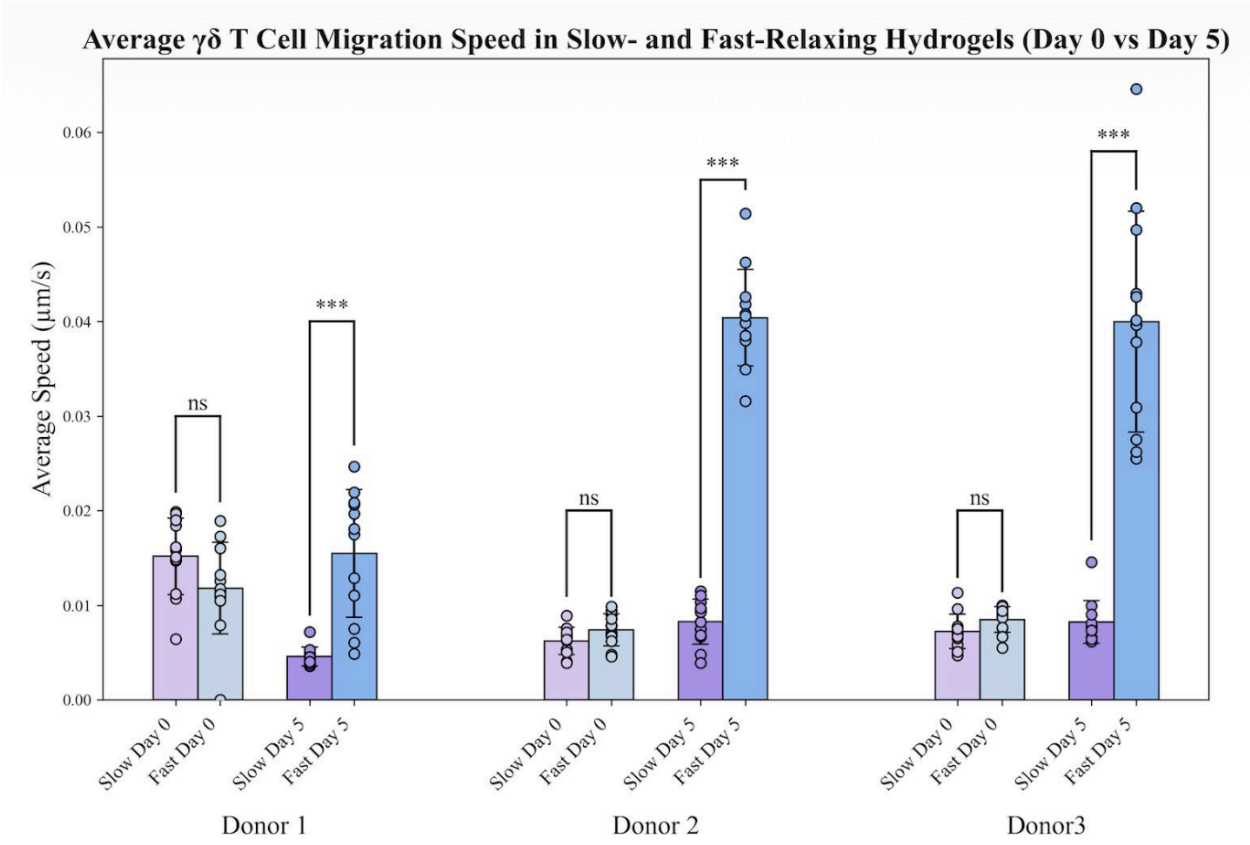

Figure 11: Average γδ T cell migration speed in slow- and fast-relaxing hydrogels on Day 0 and Day 5. Bars represent mean cell speed (μm/s) ± SD with pen circles represent each tile of gel photographed on the confocal. For each donor, γδ T cells encapsulated in fast-relaxing hydrogels exhibit significantly higher migration speeds than those in slow-relaxing hydrogels by Day 5, while no significant differences are observed on Day 0 (ns). ***$p < 0.001$ by statistical comparison between indicated conditions.

By Day 5, however, clear differences emerged between the two matrix conditions. γδ T cells embedded within fast-relaxing hydrogels exhibited substantially higher average speeds and greater MSD values, suggesting increased motility and spatial distribution within the hydrogel. This was most evident in Donor 2 and Donor 3, where migration speed increased by three fold in fast-relaxing gels and mean squared displacement increased by ten fold in slow-relaxing gels.

Although γδ T cells in slow-relaxing hydrogels exhibited measurable average speeds, their MSD values remained relatively low. This suggests that while cells may still move locally within the matrix, much of this motion likely represents oscillatory or back-and-forth movement

around a confined region, rather than sustained directional migration that results in net displacement across the hydrogel. In contrast, the higher MSD observed in fast-relaxing matrices indicates that cells are able to move throughout and away from their origins, which is consistent with enhanced migration through the matrix.

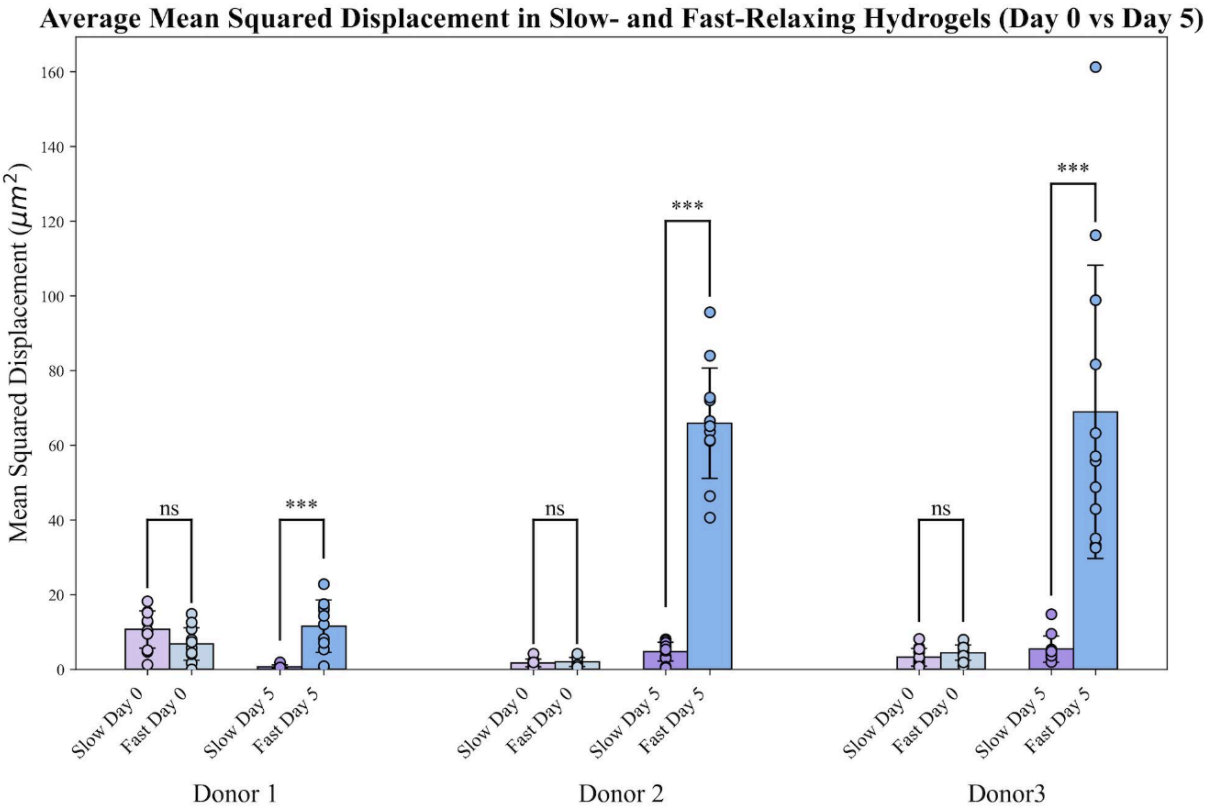

Figure 12: Average γδ T cell migration speed in slow- and fast-relaxing hydrogels on Day 0 and Day 5. Bars represent mean cell speed (μm/s) ± SD with pen circles represent each tile of gel photographed on the confocal. For each donor, γδ T cells encapsulated in fast-relaxing hydrogels exhibit significantly higher migration speeds than those in slow-relaxing hydrogels by Day 5, while no significant differences are observed on Day 0 (ns). ***$p < 0.001$ by statistical comparison between indicated conditions.

5.5 Expression of tissue-resident associated markers

To understand the effects of slow- or fast-relaxing gels on γδ T cell phenotypes, we examined the expression of PD1, DNAM1, NKG2D, and CD11a. The percentage of cells

expressing PD1, DNAM1, NKG2D, and CD11a was quantified for three independent donors at baseline (Day 0) and following 5 days of encapsulation under each viscoelastic condition. Overall, both slow- and fast-relaxing gels increased PD1 expression in all three donors relative to baseline. In two of the three donors, the slow-relaxing gels induced a larger increase in the

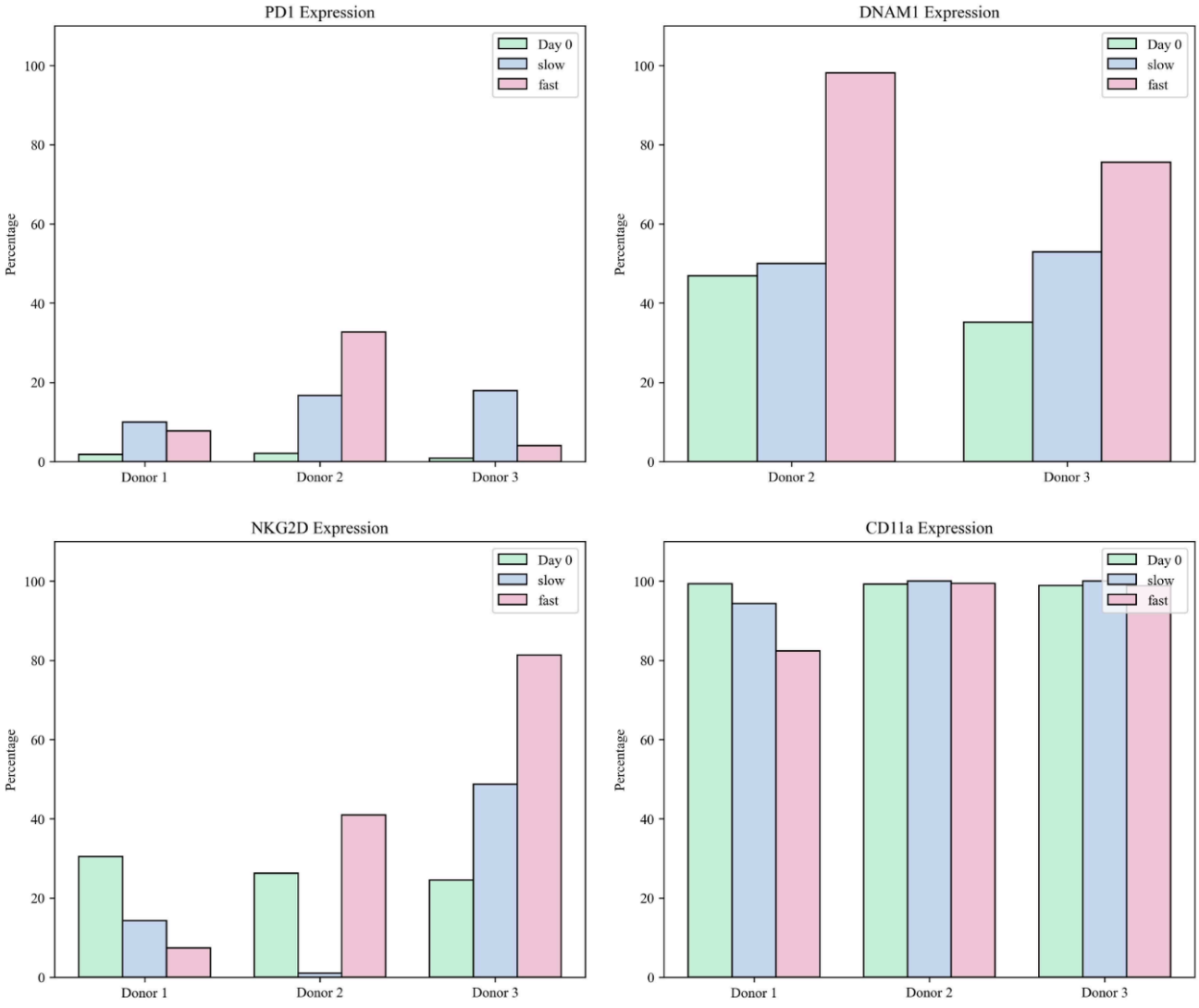

Figure 13: Expression of tissue-residency markers from three donors at baseline (Day 0) and after culture under slow- and fast-relaxing hydrogels

percentage of $PD1^+$ cells than the fast-relaxing gels, suggesting that more slowly relaxing substrates may promote a tissue-resident phenotype of γδ T cells.

For DNAM1, expression tended to be highest on fast-relaxing gels, whereas slow-relaxing gels induced only a small increase relative to Day 0. NKG2D expression showed a similar trend, with the highest percentages of $NKG2D^+$ cells generally observed on fast-relaxing gels. Donor 1 however, displayed a more complex pattern that did not follow this trend. In contrast, CD11a expression was high and relatively unchanged across all conditions and donors. Future studies will therefore incorporate geometric mean fluorescence intensity or alternative quantitative measures of CD11a expression.

These data collectively suggest that matrix relaxation properties can differentially modulate the expression of activating and inhibitory receptors on γδ T cells, with PD1 preferentially upregulated on slow-relaxing gels and DNAM1/NKG2D more strongly induced on fast-relaxing gels. However, given the small number of donors analyzed and the donor-to-donor variability observed, particularly for NKG2D, these findings should be considered preliminary. Expanding the cohort size and integrating more detailed phenotypic analyses will be essential to determine the robustness and functional significance of these mechanosensitive changes in γδ T cell receptor expression.

Chapter Six: Discussion

6.1 Conclusion

This thesis investigates how the viscoelastic properties of a three-dimensional collagen I hydrogel regulate γδ T cell migration and phenotype. Using a tunable hydrogel platform, γδ T cells were encapsulated in slow- versus fast-relaxing matrices. They were then assessed their motility through live cell confocal imaging and their receptor expression by flow cytometry.

Through the confocal imaging component of this project, it was revealed that γδ T cells adopt an amoeboid-like migration pattern within hydrogels. They elongate, extend, retract membrane protrusions as they probe and migrate throughout their environment. This behavior suggests action remodeling and matrix interaction may occur during migration. Furthermore, quantitative tracking demonstrated that on day 0, all γδ T cells remained within approximately 25 μm of their starting positions, regardless of whether they were encapsulated in a slow-relaxing or fast-relaxing hydrogel. However, by day 5, while γδ T cell migration still remained limited in slow-relaxing hydrogels, fast-relaxing hydrogels supported higher average speeds and increased mean squared displacement, indicating more efficient exploration of the surrounding matrix.

Phenotypically, the fraction of $PD1^+$ γδ T cells increased across all donors after encapsulation in both viscoelastic conditions, with slow-relaxing gels producing a larger PD1 upregulation in two of three donors. This finding is consistent with the idea that more slow relaxing matrices may promote features associated with tissue adaptation or residency. In contrast, DNAM1 and NKG2D were generally highest in fast-relaxing gels, suggesting that mechanically permissive environments favor migratory, cytotoxic γδ T cell states. CD11a expression remained high and relatively unchanged across all conditions. Further analysis

through geometric means would be necessary to determine if there were any changes in receptor expression.

Together, this data shows that hydrogel viscoelasticy can help tune the tissue-resident state of γδ T cells. Slow-relaxing matrices bias cells toward increased PD1 expression, while fast-relaxing matrices enhance motility and the expression of cytotoxic-associated receptors. Although the study is limited by donor number, a single late time point, and reliance on a small panel of surface markers, it establishes preliminary data for understanding how γδ T cells sense and respond to their physical environment**.**

6.2 Future Work

The present study provides initial evidence that matrix viscoelasticity modulates γδ T cell phenotype and migration, however there are several limitations of this study that highlight important directions for future work. First, a more rigorous definition of a tissue-resident γδ T cell phenotype is needed. While PD-1 has shown to point to a tissue-resident state, DNAM1 and NKG2D are typically associated with cytotoxicity rather than exclusively tissue-residency. Bulk RNA sequencing could be valuable in the initial approach to capture transcriptional changes caused by the various hydrogel conditions and could identify better candidate genes and pathways that mechanically influence different γδ T cell phenotypes.

Second, our assessment of γδ T cell movement was restricted to confocal imaging. To better understand the morphology of migration, it may be helpful to include acting staining and collagen staining to directly see how actin remodeling and the cell-hydrogel interactions affect migration. This will allow us to clarify the amoeboid-like movement the γδ T cells seem to employ. Furthermore, it may be helpful to stain for different γδ T cell subsets to see how subsets

whether specific populations preferentially acquire tissue-resident or migratory phenotypes in response to mechanical cues.

Third, our experiments were conducted at a single post-encapsulation time point. Adding earlier and intermediate time points (e.g., days 1–3) will clarify the kinetics of mechanical priming and receptor modulation. Exploring a broader range of viscoelastic properties and gel formulations, as well as larger hydrogel constructs that support higher cell numbers, will also be critical. For example, it may be helpful to encapsulate γδ T cells in a hydrogel more similar to the mechanical properties of the tumor rather than the lymph node. In addition, there is a need to adjust and optimize collagenase concentration and digestion protocols to reduce cell death and improve cell recovery for downstream flow cytometry.

Overall, technical and biological replications should be expanded. This thesis is based on three donors, limiting our ability to account for inter-donor variability. Screening donors for baseline memory subsets and normalizing across these populations will enable more controlled comparisons and allow us to interrogate mechanical responses within defined γδ T cell subsets.

References

Adu-Berchie, K., Brockman, J. M., Liu, Y., To, T. W., Zhang, D. K. Y., Najibi, A. J., Binenbaum, Y., Stafford, A., Dimitrakakis, N., Sobral, M. C., Dellacherie, M. O., & Mooney, D. J. (2023). Adoptive T cell transfer and host antigen-presenting cell recruitment with cryogel scaffolds promotes long-term protection against solid tumors. *Nature Communications, 14*, 3546. https://doi.org/10.1038/s41467-023-39330-7

Anderson, N. M., & Simon, M. C. (2020). The tumor microenvironment. *Current Biology, 30*(16), R921–R925. https://doi.org/10.1016/j.cub.2020.06.081

Baruch, E. N., Berg, A. L., Besser, M. J., Schachter, J., & Markel, G. (2017). Adoptive T cell therapy: An overview of obstacles and opportunities. *Cancer, 123*(11), 2154–2162. https://doi.org/10.1002/cncr.30491

Bilotta, M. T., Antignani, A., & Fitzgerald, D. J. (2022). Managing the tumor microenvironment to improve the efficacy of cancer therapy. *Frontiers in Immunology, 13*, 954992. https://doi.org/10.3389/fimmu.2022.954992

Cen, L., Liu, W., Cui, L., Zhang, W., & Cao, Y. (2008). Collagen tissue engineering: Development of novel biomaterials and applications. *Pediatric Research, 63*(5), 492–496. https://doi.org/10.1203/PDR.0b013e31816c5bc3

Cieslak, S. G., & Shahbazi, R. (2025). Gamma–delta (γδ) T cells and their immunotherapeutic potential in cancer. *Biomarker Research, 13*, 51. https://doi.org/10.1186/s40364-025-00762-6

Davey, M. S., Willcox, C. R., Baker, A. T., Hunter, S., & Willcox, B. E. (2018). Recasting human Vγ9Vδ2 T cells as professional immune sensors. *Trends in Immunology, 39*(9), 704–716. https://doi.org/10.1016/j.it.2018.07.004

Davies, D., Kamdar, S., Woolf, R. et al. PD-1 defines a distinct, functional, tissue-adapted state in Vδ1+ T cells with implications for cancer immunotherapy. Nat Cancer 5, 420–432 (2024). https://doi.org/10.1038/s43018-023-00690-0

Dhatchinamoorthy, K., Colbert, J. D., & Rock, K. L. (2021). Cancer immune evasion through loss of MHC class I antigen presentation. *Frontiers in Immunology, 12*, 636568. https://doi.org/10.3389/fimmu.2021.636568

Deseke, M., & Prinz, I. (2020). Ligand recognition by the γδ TCR and discrimination between homeostasis and stress conditions. *Cellular & Molecular Immunology, 17*(9), 914–924. https://doi.org/10.1038/s41423-020-0503-y

Dobosz, P., & Dzieciątkowski, T. (2019). The intriguing history of cancer immunotherapy. *Frontiers in Immunology, 10*, 2965. https://doi.org/10.3389/fimmu.2019.02965

Dong, R., Yang, Y., & Liu, Y. (2022). Engineering γδ T cells: Recognizing and activating on their own terms. *Frontiers in Immunology, 13*, 859774. https://doi.org/10.3389/fimmu.2022.859774

Dougé, A., El Ghazzi, N., Lemal, R., & Rouzaire, P. (2024). Adoptive T-cell therapy in solid tumors: State-of-the-art, current challenges, and upcoming improvements. *Molecular Cancer Therapeutics, 23*(3), 272–284. https://doi.org/10.1158/1535-7163.MCT-23-0310

Ershov, D., Phan, M.-S., Pylvänäinen, J. W., Rigaud, S. U., Le Blanc, L., Charles-Orszag, A., Conway, J. R. W., Laine, R. F., Roy, N. H., Bonazzi, D., Duménil, G., Jacquemet, G., & Tinevez, J.-Y. (2022). TrackMate 7: Integrating state-of-the-art segmentation algorithms into tracking pipelines. *Nature Methods, 19*(7), 829–832. https://doi.org/10.1038/s41592-022-01507-1

Escobar, G. (2025). *CAR-T cells in solid tumors: Challenges and breakthroughs*. Cell Reports

Medicine. https://doi.org/10.1016/j.xcrm.2025.102426

Fischer, M. A., Golovchenko, N. B., & Edelblum, K. L. (2020). γδ T cell migration: Separating trafficking from surveillance behaviors at barrier surfaces. *Immunological Reviews, 298*(1), 165–180. https://doi.org/10.1111/imr.12915

Hayday, A. C. (2009). γδ T cells and the lymphoid stress-surveillance response. *Immunity, 31*(2), 184–196. https://doi.org/10.1016/j.immuni.2009.08.006

Hayday, A. C. (2019). γδ T cell update: Adaptive orchestrators of immune surveillance. Nature Reviews Immunology, 19(8), 497–508. https://doi.org/10.1038/s41577-019-0173-1

He, Q., Tian, F., Xu, Y., Swamiappan, S., Zhou, Y., Zhou, Y., Hu, Z., & Peng, X. (2025). Recent advances in the development and application of cell-loaded collagen scaffolds for tissue engineering. *Bioengineering*, 12(5), 501. https://doi.org/10.3390/bioengineering12050501

Hedges, J. F., Lubick, K. J., & Jutila, M. A. (2020). Harnessing γδ T cells as natural immune modulators. *Frontiers in Immunology, 11*, 601. https://doi.org/10.3389/fimmu.2020.00601

Hu, J., Li, X., Yang, L., & Li, H. (2022). Hypoxia, a key factor in the immune microenvironment. *Biomedicine & Pharmacotherapy, 150*, 113068. https://doi.org/10.1016/j.biopha.2022.113068

Jianzhen L, Liu, Z., Ren, X., Song, S., Zhang, Y., & Wang, Y. (2025). γδT cells, a key subset of T cells for cancer immunotherapy. *Frontiers in Immunology, 16*, 1562188. https://doi.org/10.3389/fimmu.2025.1562188

Kabelitz, D., Serrano, R., Kouakanou, L., Peters, C., & Kalyan, S. (2017). Cancer immunotherapy with γδ T cells: Many paths ahead of us. *Cellular & Molecular Immunology, 14*(10), 1–10. https://pmc.ncbi.nlm.nih.gov/articles/PMC5859029/

Kabelitz, D., & He, W. (2011). γδ T cells: Cross-talk between innate and adaptive immunity. *Cellular and Molecular Life Sciences, 68*(14), 2339–2350. https://doi.org/10.1007/s00018-011-0675-0

Khan, R., Khan, M. H., & Bey, A. (2013). Use of collagen as a biomaterial: An update. *Journal of Indian Society of Periodontology, 17*(4), 539–542. https://doi.org/10.4103/0972-124X.118334

Lawand, M., Déchanet-Merville, J., & Dieu-Nosjean, M.-C. (2017). Key features of gamma-delta T-cell subsets in human diseases. *Frontiers in Immunology, 8*, 761. https://doi.org/10.3389/fimmu.2017.00761

Li, K., Cardenas-Lizana, P., Lyu, J. et al. Mechanical force regulates ligand binding and function of PD-1. Nat Commun 15, 8339 (2024). https://doi.org/10.1038/s41467-024-52565-2

Luo, X., Lv, Y., Yang, J., Long, R., Qiu, J., Deng, Y., Tang, G., Zhang, C., Li, J., & Zuo, J. (2024). Gamma delta T cells in cancer therapy: From tumor recognition to novel treatments. *Frontiers in Medicine, 11*, 1480191. https://doi.org/10.3389/fmed.2024.1480191

Meng, K. P., Majedi, F. S., Thauland, T. J., Butte, M. J., & Purtic, B. (2020). Mechanosensing through YAP controls T-cell activation and metabolism. *Journal of Experimental Medicine, 217*(8), e20191320. https://doi.org/10.1084/jem.20191320

Morotti, M., Albukhari, A., Alsaadi, A., Artibani, M., Brenton, J. D., Curbishley, S. M., Dong, T., Dustin, M. L., Hu, Z., McGranahan, N., Miller, M. L., Santana-Gonzalez, L., Seymour, L. W., Shi, T., Van Loo, P., Yau, C., White, H., Wietek, N., Church, D. N., Wedge, D. C., & Ahmed, A. A. (2021). Promises and challenges of adoptive T-cell

therapies for solid tumours. *British Journal of Cancer, 124*(11), 1759–1776. https://doi.org/10.1038/s41416-021-01353-6

Mosaffa Jahromi, A., Molavi, H., Kabelitz, D., Kalantar, K., & Meri, S. (2025). Targeting RNA-binding proteins Roquin-1 and Regnase-1 for improved cancer immunotherapy. *Frontiers in Immunology, 16*, 1563858. https://doi.org/10.3389/fimmu.2025.1563858

Moser, B., & Eberl, M. (2006). γδ T cells: An alternative type of professional APC. *Trends in Immunology, 27*(3), 112–118. https://doi.org/10.1016/j.it.2006.01.002

Murad, J. P., Christian, L., Rosa, R., Ren, Y., Buckley, A. J., Lee, E. H. J., Lopez, L. S., Park, A. K., Yang, J., Yamaguchi, Y., Trac, C., Adkins, L. N., Chang, W.-C., Martinez, C., June, C. H., Forman, S. J., Ishihara, J., Lee, J. K., Stern, L. A., & Priceman, S. J. (2025). Solid tumour CAR-T cells engineered with fusion proteins targeting PD-L1 for localized IL-12 delivery. *Nature Biomedical Engineering*. https://doi.org/10.1038/s41551-025-01509-2

Nagarsheth, N., Wicha, M. S., & Zou, W. (2017). Chemokines in the cancer microenvironment and their relevance in cancer immunotherapy. *Nature Reviews Immunology, 17*(9), 559–572. https://doi.org/10.1038/nri.2017.49

Nicol, A. J., Tokuyama, H., Mattarollo, S. R., Hagi, T., Suzuki, K., Yokokawa, K., & Nieda, M. (2011). Clinical evaluation of autologous γδ T cell-based immunotherapy for metastatic solid tumours. *British Journal of Cancer, 105*(6), 778–786. https://doi.org/10.1038/bjc.2011.293

Ng, L., Navarro, A., & Law, W.-L. (2023). Editorial: Evolving roles of piRNAs in solid tumors. *Frontiers in Oncology, 13*, 1178634. https://doi.org/10.3389/fonc.2023.1178634

Poggi, A., & Zocchi, M. R. (2014). γδ T lymphocytes as a first line of immune defense: Old and

new ways of antigen recognition and implications for cancer immunotherapy. *Frontiers in Immunology, 5*, 575. https://doi.org/10.3389/fimmu.2014.00575

Revesz, I. A., Joyce, P., Ebert, L. M., & Prestidge, C. A. (2024). Effective γδ T-cell clinical therapies: Current limitations and future directions. *Clinical & Translational Immunology, 13*, e1492. https://doi.org/10.1002/cti2.1492

Rezvani Ghomi, E., Nourbakhsh, N., Akbari Kenari, M., Zare, M., & Ramakrishna, S. (2021). Collagen-based biomaterials for biomedical applications. *Journal of Biomedical Materials Research Part B: Applied Biomaterials, 109*(12), 1986–1999. https://doi.org/10.1002/jbm.b.34881

Sakr, R. A., Nasr, A. A., Zineldin, E. I., & Gouda, M. A. (2023). Long-term survival in patients with cancers: Surveillance, epidemiology and end results–based analysis. *Sultan Qaboos University Medical Journal, 23*(3), 344–350. https://doi.org/10.18295/squmj.1.2023.002

Thirumalaivasan, N. (2025). Collagen-composite scaffolds for alveolar bone and dental tissue regeneration: Advances in material development and clinical applications—A narrative review. *Dentistry Journal, 13*(9), 396. https://doi.org/10.3390/dj13090396

Olson, D. J., & Odunsi, K. (2023). Adoptive cell therapy for nonhematologic solid tumors. *Journal of Clinical Oncology, 41*(18), 3397–3407. https://doi.org/10.1200/JCO.22.01618

Peranzoni, E., Lemoine, J., Vimeux, L., Feuillet, V., Barrin, S., Kantari-Mimoun, C., Bercovici, N., Guérin, M., Biton, J., Ouakrim, H., Régnier, F., Lupo, A., Alifano, M., Damotte, D., & Donnadieu, E. (2018). Macrophages impede CD8 T cells from reaching tumor cells and limit the efficacy of anti-PD-1 treatment. *Proceedings of the National Academy of*

Sciences of the United States of America, 115(17), E4041–E4050. https://doi.org/10.1073/pnas.1720948115

Strid, J., Sobolev, O., Zafirova, B., Polic, B., Hayday, A. (2008). Regulation of murine dendritic epidermal T cell activation by stress signals through NKG2D. *Nature Immunology, 9*(4), 395–402. https://doi.org/10.1038/ni1560

Victor Yazbeck, Erin Alesi, Jennifer Myers, Mary Helen Hackney, Laurie Cuttino, David A. Gewirtz, Chapter One - An overview of chemotoxicity and radiation toxicity in cancer therapy, Editor(s): David A. Gewirtz, Paul B. Fisher, Advances in Cancer Research, Academic Press, Volume 155, 2022, Pages 1-27, ISSN 0065-230X, ISBN 9780323900874, https://doi.org/10.1016/bs.acr.2022.03.007.

Wang, L., Geng, H., Liu, Y., Li, C., Zhang, X., & Li, S. (2023). Hot and cold tumors: Immunological features and therapeutic strategies. *MedComm, 4*(3), e343. https://doi.org/10.1002/mco2.343

Wolf, K., Müller, R., Borgmann, S., Bröcker, E.-B., & Friedl, P. (2003). Amoeboid shape change and contact guidance: T-lymphocyte crawling through fibrillar collagen is independent of matrix remodeling by MMPs and other proteases. *Blood, 102*(9), 3262–3269. https://doi.org/10.1182/blood-2002-12-3791

Wu, B., Zhang, B., Li, B., Wu, H., & Jiang, M. (2024). Cold and hot tumors: From molecular mechanisms to targeted therapy. *Signal Transduction and Targeted Therapy, 9*, 274. https://doi.org/10.1038/s41392-024-01979-x

Xia, X., Yang, Z., Lu, Q., Liu, Z., Wang, L., Du, J., Li, Y., Yang, D.-H., & Wu, S. (2024).

Reshaping the tumor immune microenvironment to improve CAR-T cell–based cancer immunotherapy. *Molecular Cancer, 23*(1), 175. https://doi.org/10.1186/s12943-024-02079-8

Xia, K., Chen, X., Wang, W., Liu, Q., Zhao, M., Ma, J., & Jia, H. (2024). Roles of mechanosensitive ion channels in immune cells. *Heliyon, 10*(1), e24876. https://doi.org/10.1016/j.heliyon.2023.e24876

Zhu, J., Li, Z., Zou, Y., Sun, Y., & Zhang, X. (2022). Advanced application of collagen-based biomaterials in tissue repair and restoration. *Journal of Leather Science and Engineering, 4*, 30. https://doi.org/10.1186/s42825-022-00102-6

Appendix

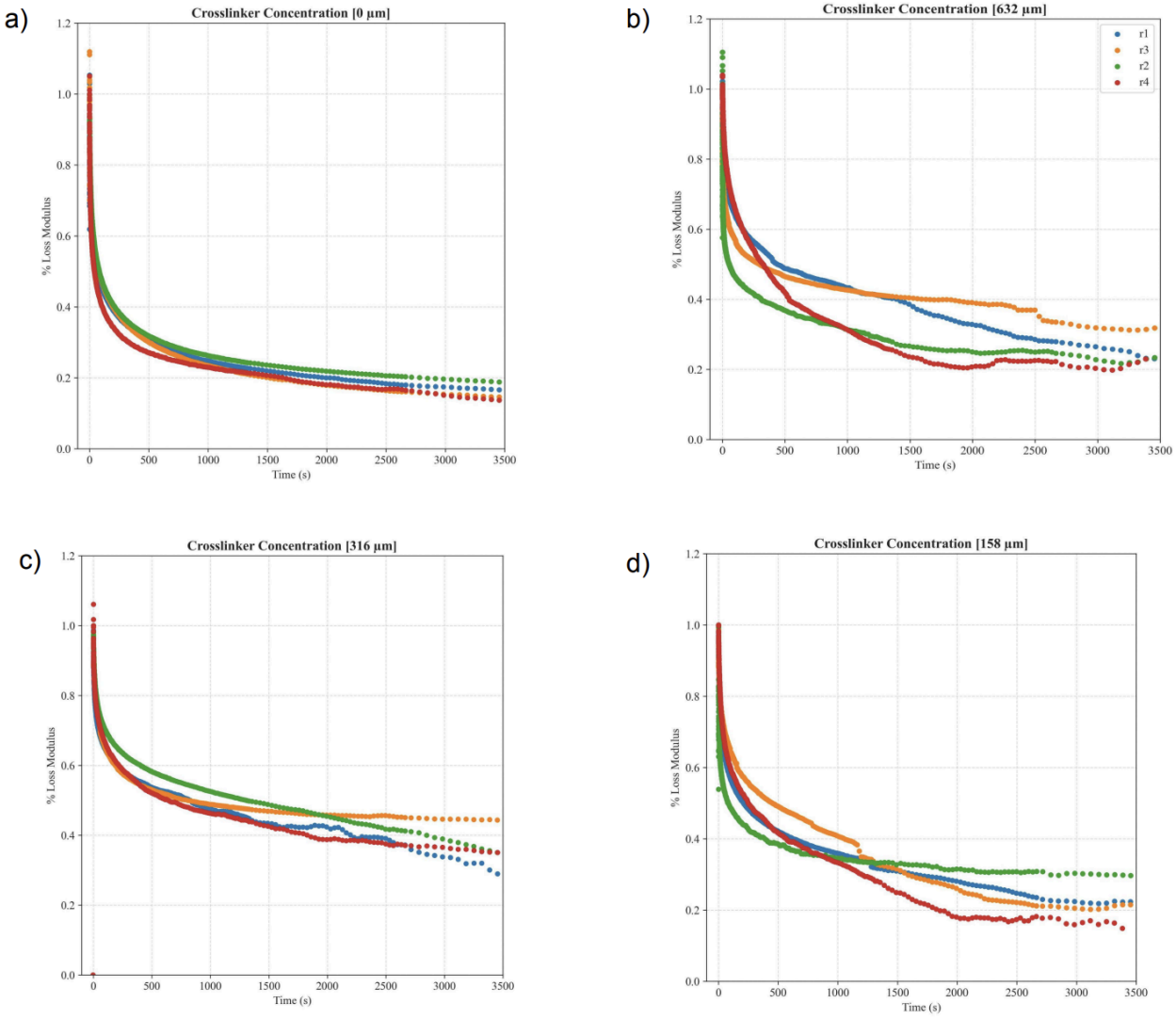

Supplement 1: Stress Relaxation Profiles indicate that viscoelasticity can be tuned based on crosslinker concentration a-d) Shear stress relaxation profiles of different crosslinker concentration. Crosslinker concentration can finetune the viscoelastic properties of hydrogels.

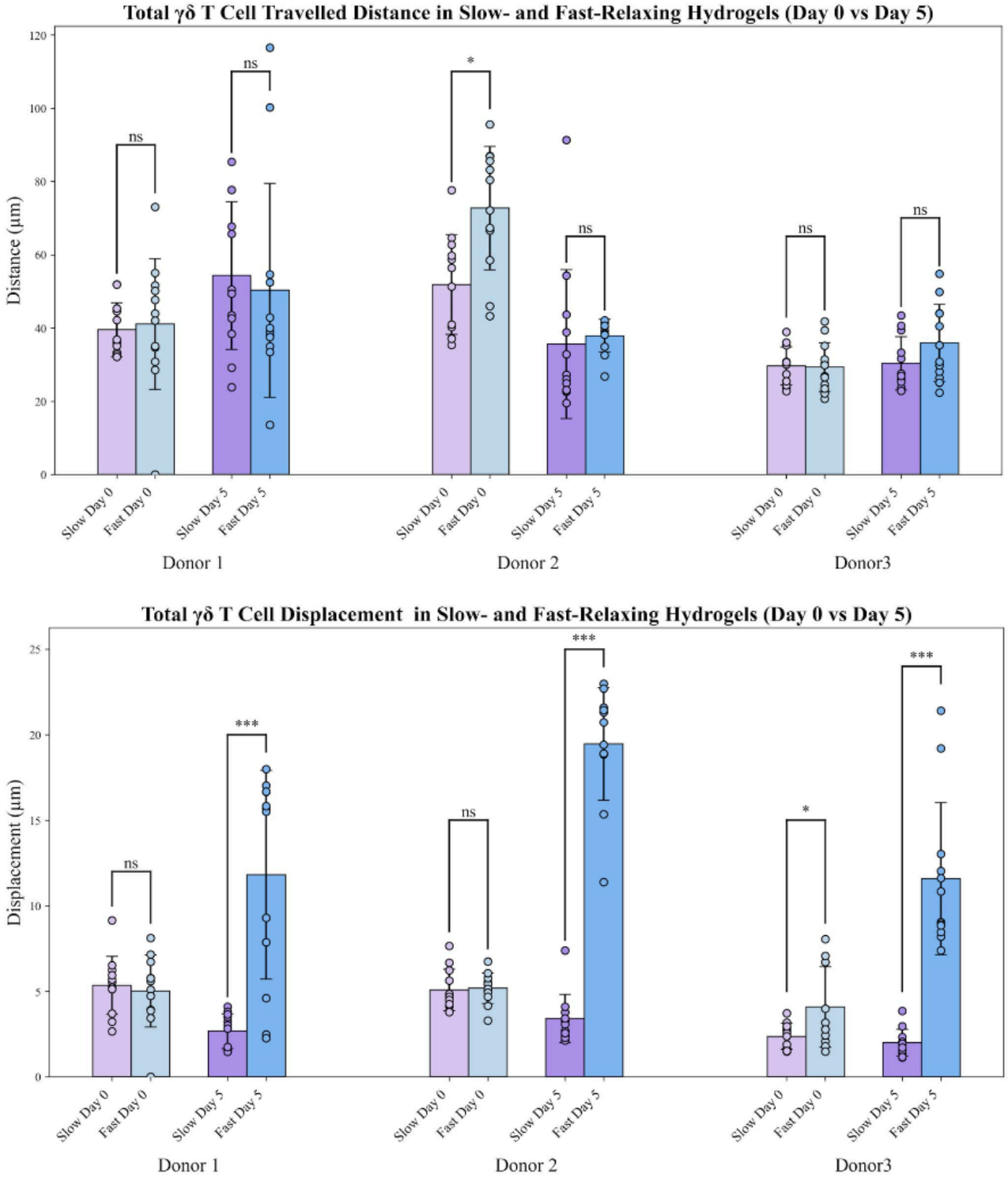

S2: γδ T cell motility in slow- and fast-relaxing hydrogels over time.
(Top) Total γδ T cell travelled distance and (Bottom) net displacement in slow- versus fast-relaxing hydrogels at Day 0 and Day 5 for three independent donors. ns: not significant, *$p < 0.05$, ***$p < 0.001$.

Supplementary Table 1: Donor 1 Day 0

Tile	Total Displacement (microns)	Total Distance (microns)	Mean Squared Displacement (microns²)	Average Speed (microns/ms)	Std Error Speed (microns/ms)
slow1-1	2.660513038	33.3601732	1.21882236	0.00641121	0.00263766
slow1-2	5.224612173	32.7270286	4.67219554	0.0106948	0.00426371
slow1-3	9.140132335	51.9061107	15.4379663	0.01968415	0.00782038
slow1-4	5.68765778	36.02009	10.4028402	0.01472479	0.00839548
slow1-5	3.700363682	35.1611186	9.47399789	0.01486278	0.00635181
slow1-6	3.223571716	51.8439954	5.11754815	0.01120914	0.00537705
slow1-7	5.951255839	42.210697	13.0317941	0.01840421	0.00990648
slow1-8	5.128813689	32.1560636	9.55297778	0.01510409	0.00824116
slow1-9	6.516893181	36.8094621	15.1745188	0.01900298	0.00645389
slow1-10	5.126810543	32.3330512	12.7142825	0.01583221	0.00641708
slow1-11	6.242381155	44.6107428	18.260307	0.01987481	0.009813
slow1-12	5.533953235	45.3393275	12.6346135	0.01613585	0.00750539
fast1-1	5.105558346	34.7030947	7.1991181	0.01089423	0.00628789
fast1-2	4.73230973	42.0121864	10.8228604	0.01603668	0.00715928
fast1-3	5.589101013	47.6774558	7.9946777	0.01319128	0.00828068
fast1-4	3.916118078	30.828071	7.33390955	0.01175167	0.00682615
fast1-5	6.719165762	55.0442438	14.8517755	0.01890536	0.00865879
fast1-6	3.866895223	35.0694593	12.5217257	0.01727583	0.00662598
fast1-7	5.756229437	50.1587821	4.07965143	0.01114685	0.00356469
fast1-8	0	0	0	0	0
fast1-9	3.430643229	28.5354439	4.40661012	0.01050277	0.00448088
fast1-10	5.772002889	51.6318159	4.52636788	0.01140316	0.00577928
fast1-11	8.120147351	73.0517567	1.70387147	0.00786587	0.00421002
fast1-12	7.156442217	43.9827066	5.73056337	0.01257317	0.00651228

Supplementary Table 2: Donor 1 Day 5

Tile	Total Displacement (microns)	Total Distance (microns)	Mean Squared Displacement (microns²)	Average Speed (microns/ms)	Std Error Speed (microns/ms)
slow1-1	1.5342197	77.6851506	0.66660244	0.00492484	0.00280706
slow1-2	1.5342197	77.6851506	0.66660244	0.00492484	0.00280706
slow1-3	4.09388969	43.5107572	0.95764712	0.0048241	0.00279079
slow1-4	2.82552336	38.3660976	0.9178723	0.00529391	0.00177474
slow1-5	3.506996	85.3465755	0.32680032	0.00358575	0.00224279
slow1-6	3.81085081	67.7007183	0.37132629	0.00381231	0.0018013
slow1-7	1.46644328	29.1786204	0.57295907	0.00452591	0.00186905
slow1-8	1.74098529	42.6729843	1.8566693	0.00718834	0.00213183
slow1-9	3.66008904	65.7303493	0.48590352	0.00402583	0.0026688
slow1-10	3.24249914	50.4730738	0.33226214	0.00358007	0.00200851
slow1-11	1.60108358	23.8341243	0.50018286	0.0042569	0.00154535
slow1-12	3.01799353	49.3851884	0.40818489	0.00396434	0.00198873
fast1-1	9.29201649	54.655153	8.14191787	0.01289073	0.00729172
fast1-2	4.60249354	116.553861	0.57114613	0.00486272	0.00277033
fast1-3	2.47269741	13.5783911	5.33664123	0.00751554	0.00466055
fast1-4	7.8745423	52.4283727	7.14830054	0.01104222	0.00711803
fast1-5	2.25366671	100.217688	0.87350409	0.0060489	0.0033521
fast1-6	17.9823646	38.8904243	22.8368271	0.02464481	0.01136068
fast1-7	16.6647753	42.8887131	12.057478	0.01746628	0.01108946
fast1-8	15.8332963	37.5707393	17.4837269	0.02194917	0.01077131
fast1-9	16.6766295	39.9926029	14.3486633	0.01808941	0.00890904
fast1-10	15.6957418	38.0348192	16.7905226	0.01968281	0.00945354
fast1-11	15.5075435	35.0085982	15.8985968	0.02063717	0.01264097
fast1-12	17.0306797	33.4684811	16.2532821	0.02086283	0.01087209

Supplementary Table 3: Donor 2 Day 0

Tile	Total Displacement (microns)	Total Distance (microns)	Mean Squared Displacement (microns²)	Average Speed (microns/ms)	Std Error Speed (microns/ms)
slow1-1	7.65862205	51.303044	0.43860937	0.00402498	0.0024146
slow1-2	5.63432973	62.7746583	1.19669426	0.00642185	0.00364902
slow1-3	4.6811838	35.3452498	1.15638968	0.00531534	0.00306432
slow1-4	4.50509809	37.1518212	1.64786109	0.00711721	0.00334369
slow1-5	3.82273585	40.2156381	1.1368973	0.00630247	0.00355619
slow1-6	6.23103865	77.5957598	0.69273454	0.00503704	0.00306948
slow1-7	6.67523284	56.4327299	0.45702416	0.00389961	0.00263513
slow1-8	4.24747015	37.0470957	4.19094354	0.0088905	0.00456666
slow1-9	3.7821833	40.9017674	1.92914017	0.00635664	0.0031433
slow1-10	4.74909589	64.6262803	2.12553676	0.00681107	0.0042626
slow1-11	4.13176375	58.7161006	2.35359941	0.00756533	0.00314936
slow1-12	4.84945604	59.7020704	2.14860203	0.00677362	0.00425379
fast1-1	3.29465252	46.0036489	3.67647899	0.00896076	0.00426635
fast1-2	4.14849827	72.1455665	1.70482058	0.00778922	0.00408996
fast1-3	5.42846499	80.426757	1.19481708	0.00671266	0.00349013
fast1-4	5.14469568	86.8238346	1.57879288	0.00789572	0.00384056
fast1-5	5.78215784	85.5922894	2.92979768	0.00854872	0.00470948
fast1-6	4.92833595	43.2683053	4.17805212	0.00986766	0.00521666
fast1-7	4.67625939	66.6326075	0.67654414	0.0047605	0.00294236
fast1-8	6.05678934	58.4756943	1.18652086	0.00621311	0.00331745
fast1-9	6.74809454	67.3416832	0.58210892	0.00456765	0.00304224
fast1-10	5.37526754	95.5550252	1.43140377	0.00708398	0.0037469
fast1-11	5.55321967	86.9973125	1.27994145	0.00693757	0.0036486
fast1-12	5.01129907	83.1765836	3.08888787	0.0094139	0.00518666

Supplementary Table 4: Donor 2 Day 5

Tile	Total Displacement (microns)	Total Distance (microns)	Mean Squared Displacement (microns²)	Average Speed (microns/ms)	Std Error Speed (microns/ms)
slow1-1	3.78848662	27.2603073	8.01700058	0.01031031	0.00684873
slow1-2	2.41058305	22.5971588	7.65000039	0.00941584	0.00473196
slow1-3	2.29316856	24.905573	3.0330302	0.00683982	0.00344827
slow1-4	2.56432382	22.9894112	5.04312022	0.00822591	0.00450423
slow1-5	3.26810341	54.3152773	0.76407039	0.00479793	0.00272608
slow1-6	7.38818164	91.3187831	0.43512137	0.0039101	0.00286988
slow1-7	3.07943291	23.0575261	7.1045095	0.0092568	0.00606021
slow1-8	3.4144766	32.8359253	6.18965043	0.01102376	0.0063704
slow1-9	4.10857718	38.8435155	5.38207685	0.00969427	0.00601821
slow1-10	2.1319508	19.5092723	3.05263936	0.00667124	0.00362859
slow1-11	3.77562123	43.6761423	6.26100505	0.0114716	0.00640354
slow1-12	2.688885	26.0016263	3.45605615	0.00746844	0.0038251
fast1-1	18.8480121	40.3198386	63.6704476	0.03985661	0.01964756
fast1-2	21.5861265	41.51092	72.7480462	0.04262806	0.02055098
fast1-3	22.9903619	41.403848	66.5610781	0.04080582	0.02129219
fast1-4	21.3025534	42.1215119	65.1083292	0.04060078	0.0208804
fast1-5	19.4207234	34.8760385	83.9936176	0.04626367	0.01931298
fast1-6	18.8971229	38.1542162	61.336562	0.03848879	0.01944818
fast1-7	22.6992238	40.6148054	95.6502061	0.0514101	0.02047116
fast1-8	21.4356003	38.439505	61.1677264	0.03798582	0.02116925
fast1-9	18.8971229	38.1542162	61.336562	0.03848879	0.01944818
fast1-10	20.7258078	39.2898033	72.0530213	0.04182685	0.02198577
fast1-11	15.3443726	26.7951898	46.4360593	0.03491489	0.01474779
fast1-12	11.380426	32.569704	40.6019943	0.03159178	0.01638773

Supplementary Table 5: Donor 3 Day 0

Tile	Total Displacement (microns)	Total Distance (microns)	Mean Squared Displacement (microns²)	Average Speed (microns/ms)	Std Error Speed (microns/ms)
slow1-1	2.72183907	29.9944598	0.68978151	0.00467966	0.00216526
slow1-2	3.16988601	23.7044809	5.9039012	0.0077616	0.00355222
slow1-3	3.72137455	30.7905958	8.11242006	0.01133542	0.00497464
slow1-4	2.87418269	22.7296429	4.61119728	0.00651037	0.00321983
slow1-5	2.55729398	36.0660247	2.03261882	0.00710447	0.00398212
slow1-6	2.37457144	27.4092855	1.38593883	0.00671942	0.002768
slow1-7	1.8970492	24.3647341	3.25794719	0.00748557	0.00394137
slow1-8	2.95350853	25.437309	5.42317875	0.00958307	0.00492796
slow1-9	1.50553344	30.6409909	0.75310263	0.00506639	0.00230046
slow1-10	1.49058272	38.9423719	0.98236599	0.00582185	0.00281046
slow1-11	1.64251349	30.0084826	2.45862928	0.00759376	0.00307794
slow1-12	1.47941132	35.3038291	3.09827393	0.00709651	0.00293571
fast1-1	3.8558261	23.6913054	14.7886306	0.01454108	0.00586618
fast1-2	2.96409266	23.5891529	9.52003205	0.00993547	0.00706224
fast1-3	1.91634403	27.5822477	3.94091982	0.00736713	0.00476414
fast1-4	1.53863674	39.3979566	4.27981981	0.00657554	0.00309505
fast1-5	2.04094033	25.3274204	3.27122983	0.00811275	0.0045941
fast1-6	1.12962532	40.6556219	2.02136581	0.00615178	0.0033612
fast1-7	1.94366131	43.420315	5.15953871	0.00902473	0.00605327
fast1-8	1.15890242	26.9001215	3.66980063	0.00640403	0.00313253
fast1-9	1.71861765	22.8347716	4.78694158	0.00732697	0.00517091
fast1-10	1.97222701	26.0340169	5.36518641	0.00774556	0.00424187
fast1-11	1.39968169	31.621345	3.38016749	0.00729117	0.00360488
fast1-12	2.32005498	33.2539247	4.49677136	0.00795875	0.00570204

Supplementary Table 6: Donor 3 Day 5

Tile	Total Displacement (microns)	Total Distance (microns)	Mean Squared Displacement (microns²)	Average Speed (microns/ms)	Std Error Speed (microns/ms)
slow1-1	6.70495319	41.7561904	4.17155368	0.00999868	0.00347521
slow1-2	6.70091017	30.2510393	3.84125356	0.0087547	0.00458476
slow1-3	3.98161599	26.8712019	4.49521875	0.00868792	0.00441328
slow1-4	7.07661199	39.3713118	2.55881351	0.00759601	0.00312862
slow1-5	3.17966777	24.5697313	0.97388523	0.00549581	0.00259171
slow1-6	8.04475517	31.4031308	7.93266439	0.00987288	0.00550036
slow1-7	2.78039559	26.5787695	5.83815341	0.00940667	0.00580558
slow1-8	1.79373733	23.485923	3.66873851	0.00763727	0.00330009
slow1-9	1.47779465	29.855275	1.88915173	0.00668066	0.00313118
slow1-10	2.79638495	35.117752	6.22039638	0.00893377	0.00349926
slow1-11	2.07161111	20.6503755	6.21175793	0.00959104	0.00408117
slow1-12	2.4288878	22.1154108	5.50872376	0.00915166	0.0050356
fast1-1	12.0325852	26.3691588	55.8432998	0.03964237	0.01340207
fast1-2	8.19558347	54.8095878	161.314942	0.0645898	0.02242556
fast1-3	13.0218132	28.1333641	63.296033	0.04262855	0.01442313
fast1-4	7.38319023	49.8134774	116.254823	0.05202261	0.01962936
fast1-5	10.8442294	25.1107717	57.0726031	0.0378265	0.01181409
fast1-6	8.95019893	35.2945453	42.9645203	0.03090922	0.01131268
fast1-7	11.615253	40.5063287	33.2134837	0.0255063	0.01219875
fast1-8	8.46993685	29.8220433	35.1071577	0.02752417	0.0111529
fast1-9	8.85201231	30.8156742	32.5908559	0.02622393	0.01188827
fast1-10	9.04553095	22.3809428	48.7794113	0.04015161	0.00742904
fast1-11	21.4091604	44.0605618	98.8638224	0.04971601	0.02236882
fast1-12	19.1949516	43.9860566	81.7083553	0.04293482	0.02049377

Links to External Video Supplements:

Donor 1 γδ T cell Migration Video Fast-Relaxing Hydrogel

Donor 1 γδ T cell Migration Video Slow-Relaxing Hydrogel

Donor 2 γδ T cell Migration Video Fast-Relaxing Hydrogel

Links to Python Files Used for Image Analysis and Statistical Tests

Jupyter Notebook: Python Files